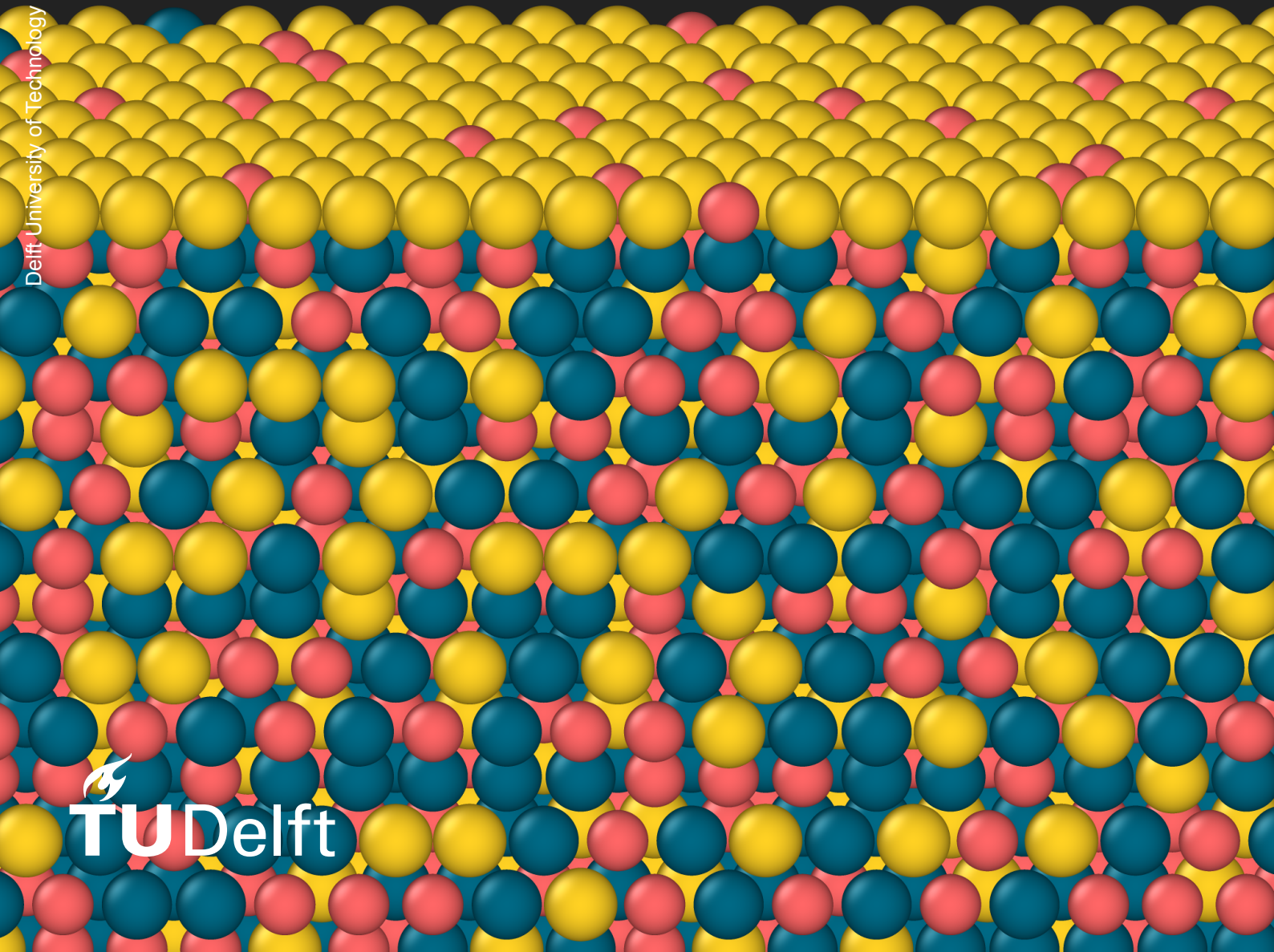


Surface segregation in Pd-based ternary alloys

Modelling surface segregation in ternary alloys using Miedema's model and Monte Carlo simulations

J.I.Postma



Surface segregation in Pd-based ternary alloys

Modelling surface segregation in ternary alloys
using Miedema's model and Monte Carlo
simulations

by

J.I. Postma

To obtain the degree of Master of Science
at the Delft University of Technology,
to be defended publicly on Tuesday July 20, 2021 at 10:00 AM.

Student number: 4633237
Project duration: September 2020 – July 2021
Thesis committee: Prof. Dr. A. Böttger, TU Delft
Dr. A. Ferrari, TU Delft
Prof. Dr. M. H. F. Sluiter, TU Delft

An electronic version of this thesis is available at <http://repository.tudelft.nl/>.

Acknowledgments

During the Covid-19 pandemic it has been difficult for everyone to make work work I believe. But I thoroughly enjoyed my thesis project as I discovered my interest into research. However, I am convinced that it has been made a much more pleasant experience mostly because of the people that have surrounded me in the past year.

To start off with, Amarante Böttger, I am very grateful for your support. The meetings that we had always provided me with new insights and have thought me a lot. Furthermore, the rate at which I could get feedback on results or would receive papers that would guide me in the right direction made the entire thesis project go effortless. Secondly, Alberto Ferrari, I honestly believe I couldn't have wished for anything more in a supervisor. You were always happy to help and the hours that you spent sitting down with me to teach me how to use density functional theory on a supercomputer, improving my research skills and discussing my future career are all appreciated more than what I could put into words.

On a more personal note, I would like to thank my housemates with whom I have become close friends with over the past year. Thirza, thank you for supporting me and the endless hours that we spent together studying made everything much more pleasant and efficient. Lastly, I would like to thank my parents, brother and sister, whom have always told me to keep pursuing whatever I enjoyed most, supported me throughout this entire journey and have lead me to this path.

*J.I.Postma
Delft, July 2021*

Abstract

Surface compositions play a predominant role in the efficiency and lifetime of membranes and catalysts. The surface composition can change during operation due to segregation, thus controlling and predicting the surface composition is essential. Computational modeling can aid in predicting the alloy's stability, along with designing surface alloys and near-surface alloys which can outperform existing catalysts. A computational model to predict surface segregation in ternary alloys is developed. The model is based on Miedema's semi-empirical model that is used to predict mixing enthalpies. The segregation enthalpy is parameterized to describe pairwise interactions between nearest-neighbours and then used in Monte Carlo simulations. Monte Carlo simulations enable to predict short-range ordering in the surface and subsurfaces; both affect the performance of a material as a catalyst. The computational model obtained in this work is able to screen through a vast range of alloy compositions and can qualitatively predict the alloy's stability in a gas environment. In this thesis the model is applied to design a novel ternary Pd-based material for membranes that can be used to separate hydrogen from a gas mixture. Addition of specific amounts of Cu and Zr to Pd results in a material with reduced H₂S poisoning as compared to a pure Pd surface as well as an enhanced permeability. The computational model obtained in this work allows to systematically assess the composition of ternary surface alloys and near-surface alloys and is a large improvement over the trial and error approaches currently used.

Contents

Preface	i
Abstract	ii
Nomenclature	iv
List of Figures	v
List of Tables	vi
1 Introduction	1
1.1 Effect of alloying elements on Pd-based hydrogen separation membranes	2
1.2 Computational background for surface segregation	4
1.3 Surface segregation in binary alloys	5
1.4 Surface segregation in ternary alloys	11
1.5 Research purpose	15
2 Methodology	16
2.1 Miedema's model for mixing enthalpy	16
2.2 Monte Carlo simulations	17
2.3 Computational model for binary alloys	18
2.4 Computational model for ternary alloys	22
2.5 Density functional theory for hydrogen adsorption energies	24
2.6 Thermo-Calc for calculation of phase diagrams	25
3 Verification against literature	26
3.1 Surface segregation in binary alloys	26
3.2 Surface segregation in ternary alloys	33
4 Designing surface alloys	38
5 Conclusion	42
5.1 Limitations of the computational model	43
6 Recommendations	44
References	51
A Hydrogen adsorption energies	52
B Python script for surface segregation	54
C Data required for python script	55
D Python script to process surface segregation	57

Nomenclature

Abbreviations

Abbreviation	Definition
AES	Auger electron spectroscopy
CALPHAD	Calculation of Phase Diagrams
DFT	Density functional theory
EAM	Embedded atom model
ISS	Ion scattering spectroscopy
LEED	Low-energy electron diffraction
LEIS	Low-energy ion scattering spectroscopy
LM	Langmuir-McLean
MC	Monte Carlo
MEAM	Modified embedded atom model
NSA	Near surface alloy
SA	Surface alloy
SRO	Short-range ordering
SEM	Scanning electron microscope
STM	Scanning-tunneling microscopy
TB	Tight binding
XPS	X-ray photoelectron spectroscopy

List of Figures

1.1	Schematic surface segregation	1
1.2	Mechanism of permeation of hydrogen through a metal membrane	2
1.3	Oscillatory segregation calculated for Pd-Ni	5
1.4	Short-range ordering	5
1.5	Pd-Cu phase diagram	9
1.6	Composition spread alloy film of Pd-Cu-Au	12
1.7	Phase diagram of Pd-Cu-Au at 823 K	12
2.1	Possible atomic switches in a slab	19
2.2	Example of elastic drift as a result of a pairwise elastic energy term	20
2.3	Hydrogen adsorbed on fcc position	21
3.1	Segregation of Pd-alloys in vacuum at 600K from this work	28
3.2	Pd-Ni segregation at 600K compared to Zhao et al. [69]	29
3.3	Surface segregation as a function of temperature	29
3.4	Short-range ordering in Pd ₆₇ Ag ₃₃ at 0 K in vacuum for the top four atomic layers	31
3.5	Surface segregation in Pd-alloys with a monolayer hydrogen adsorbed at 600K	32
3.6	Predicted atomic fraction at the surface in Pd ₅₀ Cu ₁₀ La ₄₀ at 600 K in vacuum	34
3.7	Ternary diagrams showing excess surface segregation in Pd-Cu-Au	35
3.8	Predicted excess atomic fraction at the surface in Pd-Cu-Au at 600 K	35
4.1	Approach to tailor the surface composition of a ternary alloy	38
4.2	Approach to find transition metal that can improve the permeability of the Pd-Cu alloy	39
4.3	Phase diagram of Pd-Cu-Zr at 600 K, 800 K and 1000 K	40
4.4	Predicted excess atomic fraction at the surface of Pd-Cu-Zr at 600 K in vacuum and a hydrogen atmosphere	40
4.5	Segregation of Pd ₄₈ Cu ₄₂ Zr ₁₀	41

List of Tables

1.1	Experimental surface segregation in Pd-Ag in vacuum by various authors	6
1.2	Computational surface segregation in Pd-Ag in vacuum by various authors	7
1.3	Experimental surface segregation in Pd-Au in vacuum by various authors	8
1.4	Computational surface segregation in Pd-Au in vacuum by various authors	8
1.5	Experimental surface segregation in Pd-Cu in vacuum by various authors	10
1.6	Computational surface segregation in Pd-Cu in vacuum by various authors	10
1.7	Experimental surface segregation in Pd-Ni in vacuum by various authors	11
1.8	Computational surface segregation in Pd-Ni in vacuum by various authors	11
1.9	Reported segregation of Pd-Ag-Cu by Zhao et al. [103]	13
1.10	Reported segregation of Pd-Cu-Mo by Zhao et al. [103]	14
2.1	Hydrogen adsorption energies computed with DFT and compared against literature . . .	25
3.1	Surface segregation in five alloys in vacuum at 600 K from compared to this work	26
3.2	Surface segregation reported in literature compared to the predictions from this work . .	30
3.3	Reported segregation of Pd-Ag-Cu from Zhao et al. compared to this work	36
3.4	Reported segregation of Pd-Cu-Mo from Zhao et al. compared to this work	37
3.5	Surface segregation predicted by Yu et al. in four Pd-Pt-Rh compared to this work . . .	37
A.1	Hydrogen adsorption energies computed using DFT and compared against literature . .	53

Introduction

Surface segregation is of great importance as the catalytic activity is mostly determined by the surface layer [1], [2]. The surface composition of alloys can change during operation [3]. One or multiple elements can be enriched on the surface through a process called surface segregation, as shown in figure 1.1. Even minute changes to the composition of the surface layer or near-surface region can drastically affect the catalytic properties [2], [4]–[10]. Therefore, many applications require a control over the surface composition. Examples include the production of polyethylene [11], controlling corrosion [12], catalysts for the production of hydrogen and electrodes for CO₂ conversion [13]. Furthermore, controlling the surface segregation can lead to improved solar cells, light-emitting diodes, gas sensors, thin film transistors and more [14]. The different composition of the surface layer is known as a surface alloy (SA). Similarly, a different composition in the near-surface region is known as a near-surface alloy (NSA). These SA's and NSA's can be designed in such a way that they outperform existing catalysts [4]. Thus, controlling and being able to predict the surface composition is of paramount importance to find multicomponent alloys with improved properties. Traditionally these alloys are optimized by trial and error. A more systematic computational approach can reduce both the time and cost of optimizing SA's and NSA's.

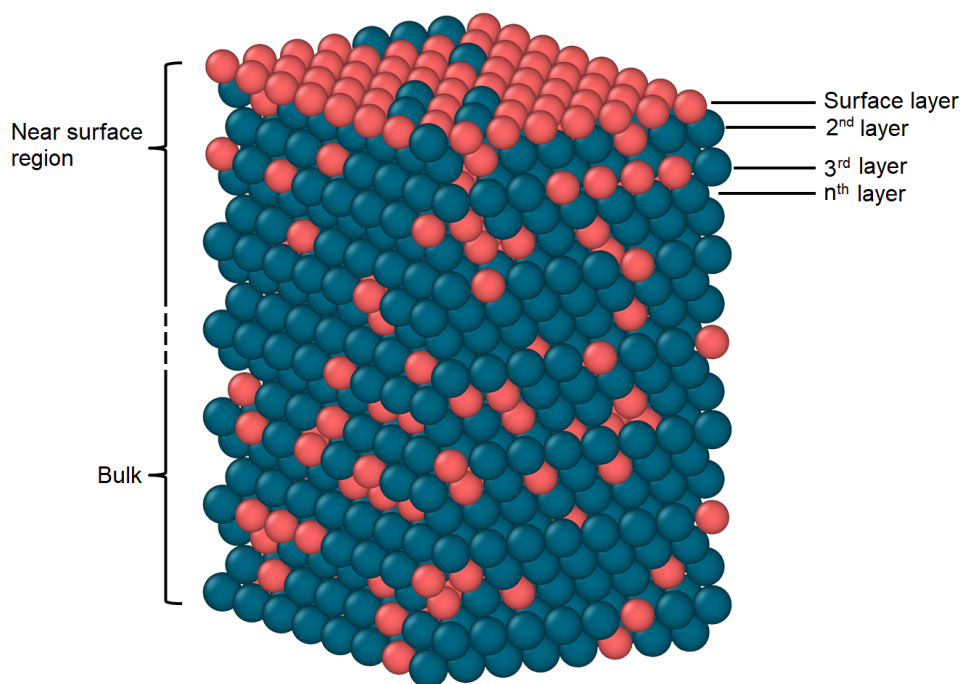


Figure 1.1: Segregation of red atoms to the surface layer.

It is more clear than ever that fossil fuels will not have a predominant role as an energy carrier for our future energy and transport systems. The drive towards a hydrogen economy has a great potential to reduce the emission of greenhouse gases. However, certain challenges have to be overcome in order to make the hydrogen economy a more realistic option. One of these challenges is the purification of hydrogen. In many applications, such as general industrial applications, hydrogenation, and water chemistry high purity (>99.95%) hydrogen is needed [15]. For polymer electrolyte membrane fuel cells, ultra-pure hydrogen (>99.97%) and CO concentrations ≤ 0.2 ppm are required [16]. Steam methane reforming is currently the most common method to produce hydrogen with a purity of 74% [17].

Hydrogen can be purified by using various methods, among which are metal membranes. Metal membranes can act as a selective barrier which allow certain gases to pass through while they stop others. The intrinsic selectivity of palladium membranes towards hydrogen has been studied extensively over the past decades and can help in producing ultra-pure hydrogen. The mechanism by which a Pd-membrane separates hydrogen from other gases is shown in figure 1.2. Pure Pd-membranes have numerous shortcomings, including a phase transition at a temperature below 570 K when hydrogen is absorbed, leading to embrittlement [18], [19]. Furthermore, certain molecules, such as CO and H₂S can lead to surface poisoning thereby decreasing the rate at which hydrogen can adsorb to the surface [20]. Finally, Pd is a scarce material and the demand is expected to rise [21]. Alloying the Pd-membrane with other metals can overcome these challenges [22]–[24].

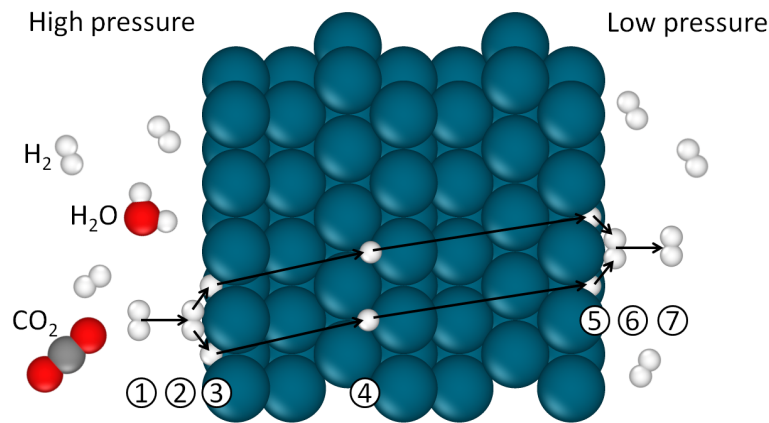


Figure 1.2: Mechanism of permeation of hydrogen through a metal membrane. 1. Diffusion in gas 2. Adsorption 3. Dissociation into atomic H on the surface 4. Diffusion through membrane 5. Recombination to molecular hydrogen 6. Desorption 7. Diffusion in gas

The aim of this thesis is to develop and verify a thermodynamic model that can predict the composition and atom arrangements in binary and ternary alloys in the (near) surface region in vacuum or a gas environment. This model will be based on an existing Miedema's model in combination with Monte Carlo (MC) simulations. The model should be able to allow relative fast screening of alloy compositions to predict the alloy's stability and to enable designing new SA and NSA systems. A focus towards hydrogen separation membranes is shown as one of the practical applications of this model.

1.1. Effect of alloying elements on Pd-based hydrogen separation membranes

Experimental and computational results on four Pd-based binary alloys (Pd-Ag, Pd-Au, Pd-Cu and Pd-Ni) are reported extensively in literature. This chapter will therefore focus on these Pd-based alloys, to compare the different computational models and the experimental results. Most of the research related to Pd-based hydrogen separation membranes focus on Pd-Ag and Pd-Cu alloys because of their improved permeability and poisoning resistance respectively.

Surface poisoning

Hydrogen dissociation of Pd-membranes can be drastically reduced as a result of surface poisoning. H₂S can adsorb on the surface and remain adsorbed, thereby decreasing the number of active sites. Pd-Cu membranes have improved poisoning resistance against H₂S and CO [25], [26]. However, Cu in the fcc phase decreases the permeability of the membrane [27]. Pd-Au membranes have improved poisoning resistance against H₂S but not against CO when compared to Pd-Cu membranes. Furthermore, adding Au increases the hydrogen solubility, leading to a larger permeability than Pd-Cu. Pd-Au membranes are however less stable in operation than Pd-Cu membranes, which causes the permeation rates to drop over time [28]. Lastly, the adsorption of hydrogen on Au is endothermic, which leads to less favourable adsorption of hydrogen to Pd-Au membranes [29].

Permeability

Permeability is defined as the ability of hydrogen to diffuse through a metal membrane. Permeability is a material constant, it is dependent on the temperature and independent of the membrane thickness [30]. Furthermore, the permeability is a function of the diffusivity which is a function of the activation energy for hydrogen diffusion and permeability is a function of the solubility which is dependent on the solution enthalpy of hydrogen. Nordlander et al. computed heats of solution of hydrogen in various transition metals and compared them to experimental results, showing that Y, Zr, Sc, Ti, Hf and La are able to improve the solubility [31].

The crystal structure and crystal plane play an important role in the permeability of a dense metal membrane. The bcc crystal structure has a larger permeability to hydrogen than fcc. Buxbaum et al. developed a Nb (bcc) membrane with a Pd (fcc) coating [32]. The Pd is necessary for the fast dissociation of hydrogen and the Nb is able to facilitate fast hydrogen permeation through the membrane. The drawback of this membrane is the segregation of Nb to the surface, which lowers the hydrogen flux. Similar experiments have been performed by Paglieri et al. for a V₉₀Pd₁₀ membrane and report an increased permeability, however their membrane cracked when it was cooled due to hydrogen embrittlement [33]. Furthermore, Paglieri et al. conclude that hydrogen embrittlement increases with an increase in the solubility of hydrogen. Morreale et al. report an improved permeability and improved surface poisoning resistance of a Pd-Cu membrane in the bcc region at high temperatures [34].

Pd-Ag membranes have improved permeability and durability [35]. The permeability increases with a factor of 2-2.5 at a composition of Pd₇₆Ag₂₄ compared to pure Pd and attribute it to the lattice expansion [36]. Pd-Y has the highest reported permeability with a permeability of around 5 times that of pure Pd and around 2 times that of the Pd-Ag membranes. The improved permeability is attributed to the ~30% larger lattice size [37], [38]. Ke et al. compared the influence of the electronic structure and lattice parameter on the solubility of hydrogen in Pd-alloys using DFT and report that the solubility is mostly dependent on the electronic structure and report four correlations that lower the stability of the hydride; 1. A higher binding energy of the host alloy, 2. a deeper hydrogen band relative to the Fermi level, 3. deeper lowest s-like electrons in the valence band and 4. a deeper Pd d-band centre [39].

Hydrogen embrittlement

Pure Pd undergoes a phase change from α to β when operated at 571 K and a pressure below 20 bar [40]. The lattice parameter changes from 3.89 Å to 4.02 Å, and thus results in a ~10% volume increase. This phase change results in a distortion of the metal lattice and induces internal stresses in the lattice structure, leading to embrittlement. Operating Pd membranes below this critical temperature will increase the hydrogen embrittlement. However, operating the Pd-membrane above this temperature will make the membrane more susceptible to surface poisoning [41]. Increasing the solubility in order to improve the permeability will also reduce the resistance to hydrogen embrittlement [42]. Ag, Au, Cu, Y and Pt can decrease the critical temperature of the Pd-membrane, allowing for lower operating temperatures [17], [43], [44]. Additionally, the difference between the lattice parameter of the α to β phase also decrease, reducing the induced stresses. Sakamoto et al. report that the difference between the lattice parameters of the α to β is also reduced by addition of Ti, Zr, Nb, Ta, Pt and Ru to Pd [45].

Conclusion on the effect of alloying elements

The perfect Pd-based hydrogen membrane does not seem to exist. Instead, Pd-based hydrogen separation membranes should be designed for a specific operation. Different operations will require different priorities when it comes to hydrogen separation membranes. One alloying element can improve one property of the membrane while decreasing the performance of another property, e.g. the addition of Cu will improve the poisoning resistance while lowering the permeability. Some general conclusions on the alloying elements can be drawn. Adding Cu while staying in the fcc phase will improve the poisoning resistance [46], decrease embrittlement [47], decrease the cost but also decrease the permeability [17]. Adding Au will improve the poisoning resistance, improve the permeability [43] and decrease embrittlement [47]. Adding Ag will improve the permeability [37] and decrease embrittlement [47]. The effect of Ni on Pd-based hydrogen separation membranes is not reported well in literature.

1.2. Computational background for surface segregation

Several computational methods have been developed to describe surface segregation in binary alloys. These models compute the segregation enthalpy ΔH_{seg} at 0 K which is then used to compute the surface segregation. Density functional theory (DFT) is an ab initio method to compute the segregation enthalpy and is one of the most used computational models in materials science and is able to describe a many-body system by using functionals of the electron density. The tight binding (TB) model uses a parameterized electronic band structure and is similar to the linear combination of atomic orbitals method, which is faster but more approximate [48]. The embedded atom model (EAM) and the modified embedded atom model (MEAM) use an interatomic potential to approximate the energy between atoms [49], [50]. An alternative to these methods to compute the segregation enthalpy is the semi-empirical Miedema's model which can be used for binary and ternary alloys which contain at least one transition metal [51]. The previously reported models are computationally more intensive than Miedema's model [48], [52]. The advantage of the theoretical models is that they give a more fundamental understanding of the segregation enthalpy, whereas thermodynamic and semi-empirical models rely on experimental data.

Langmuir-McLean equation

The Langmuir-McLean (LM) equation can estimate the surface composition with the segregation enthalpy and the bulk concentrations [53]. Due its mean-field nature it assumes a perfectly random solid solution and is shown in equation 1.1.

$$\frac{\chi_{surf}^A}{1 - \chi_{surf}^A} = \frac{\chi_{bulk}^A}{1 - \chi_{bulk}^A} \exp\left(-\frac{\Delta H_{seg}}{RT}\right) \quad (1.1)$$

Where χ_{surf}^A is the surface composition of element A, χ_{bulk}^A the bulk composition of element A, R the gas constant and T the absolute temperature. For $\Delta H_{seg} > 0$ element A will segregate to the surface and for $\Delta H_{seg} < 0$ element B will segregate to the surface. An oscillating enrichment of the surface and subsurface layers is sometimes seen in experiments. An example of this oscillation is shown in figure 1.3 for the Pd-Ni system and is often the case for alloys with a negative mixing parameter. Although it is possible to predict this oscillating enrichment with the LM equation, it is not possible to predict the ordering within the layers which affects the efficiency of catalysis [4], [54].

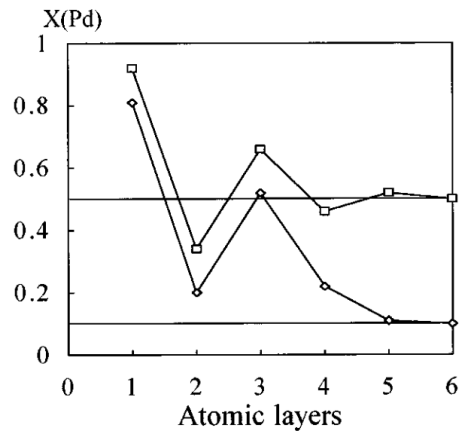


Figure 1.3: Composition depth profiles calculated for Pd-Ni by Rousset et al. at 800 K for 10 at.% and 50 at.% bulk Pd showing an oscillatory enrichment [55].

Monte Carlo simulations

Monte Carlo simulations are a different method which can be used to predict surface segregation and have the advantage that they introduce a lattice, thereby lifting the mean-field assumptions of the LM equation. Therefore, MC simulations are capable of predicting and including eventual short-range ordering (SRO) effects. MC simulations are however computationally more demanding than applying the LM equation. The effect of SRO is shown in figure 1.4. The left figure shows no SRO, the middle and right figure have the ordered region outlined in blue. Besides ordering, clustering of atoms can also occur. Above the order-disorder temperature the effect of SRO can be neglected, as shown by Ropo et al. [56], where the effect of SRO has been neglected and the results of their research agrees with the model of Ruban et al. [57], which includes SRO by using MC Simulations and other experimental results [58].

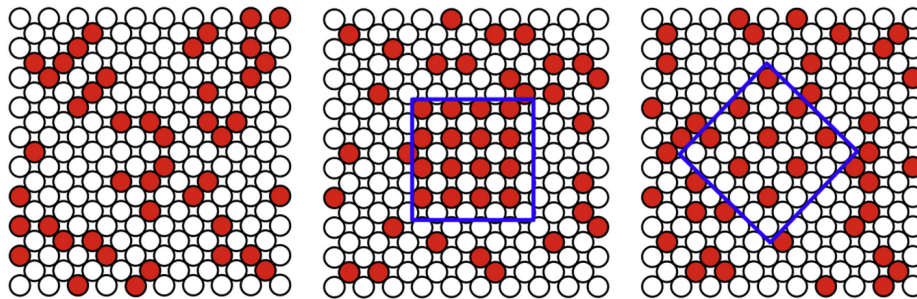


Figure 1.4: Three different types of ordering that consist of the same composition, the left figure shows no ordered regions, the middle and right figure show an ordered region outlined in blue, from Owen et al. [59].

1.3. Surface segregation in binary alloys

Extensive experimental and computational literature is available on the surface segregation in Pd-based binary alloys. The fcc phase and the crystallographic (111) plane is considered in a vacuum environment in this work, unless stated otherwise. In binary alloys, the reduction of the surface energy is the predominant driving force for surface segregation [60], [61].

Various characterization methods have been employed to obtain experimental data on surface and subsurface compositions. Low-energy ion scattering spectroscopy (LEIS), also known as ion scattering spectroscopy (ISS) is an analytical tool that provides information on the atomic composition of the surface layer [62]. Scanning-tunneling microscopy (STM) can be used to observe the surface layer. Auger electron spectroscopy (AES) and X-ray photoelectron spectroscopy (XPS) are used to study the near-surface region [63], [64] and low-energy electron diffraction (LEED) can be used to perform measurements of the surface layer and near-surface region [65]–[68].

Surface segregation in Pd-Ag

Table 1.1 shows the reported experimental data for Pd-Ag and table 1.2 shows the computational data. All authors report a segregation of Ag to the surface. Ruban et al. [57] use DFT in combination with MC to model surface segregation at the same bulk composition ($\text{Pd}_{67}\text{Ag}_{33}$) as measured by Wouda et al. (STM) [68], Noordermeer et al. [66] (AES and LEED) and Kuijers et al. (AES) [63]. The results obtained by Ruban et al. show a lower segregation of Ag compared to the experimental results of approximately 5 at.%. Ruban et al. compare their results against those of Wouda et al. and argue that this difference is due to theoretical approximations, such as neglecting lattice vibrations and relaxations in the computational model. Furthermore, the computational model was run at slightly lower temperatures (720 K and 800 K) than the measurements of Wouda et al. However, Noordermeer et al. performed their experiments at even lower temperatures (673 K) and show very similar results to those of Wouda et al. Additionally, Ropo et al. performed DFT calculations on a very similar composition ($\text{Pd}_{70}\text{Ag}_{30}$) at 600 K and report similar results to those of Ruban et al. [56]. Therefore, it is expected that the difference between the computational and experimental results is predominantly determined by the theoretical approximations.

Zhao et al. and Vurens et al. report a substantially lower surface segregation of Ag than experimental and computational results [69], [70]. Vurens et al. argue that their prediction of the lower segregation of Ag can be attributed to the large uncertainties in the input parameters used. Wouda et al. report that the high Pd concentration reported by Vurens et al. can be attributed to neglecting or underestimating the influence of the surface energies, i.e. the influence of the mixing enthalpy is overestimated [68]. Zhao et al. report that Miedema's model underestimates the surface segregation in Pd-Ag and that Calculation of Phase Diagrams (CALPHAD) gives quantitatively a better accuracy compared to experimental data. Furthermore, SRO will have an effect which is not included in the LM equation. The effect of SRO reduces with increasing temperatures where the order-disorder phase transition takes place. Ropo et al. [56] neglect the effect of SRO and their results agree with the model of Ruban et al. [57], which includes SRO by using MC Simulations. However, the temperatures used by Zhao et al. are 300 K lower and SRO could have an effect and explain the large difference between their results and the experimental results of Wouda et al. [68] and Yi et al. [67].

Wouda et al. report a depletion of Ag in the second atomic layer [68], which is confirmed by the DFT results of Ropo et al. [56], [71]. Ruban et al. report that this is an ordering effect and notice an oscillating enrichment of Ag and Pd below the surface in $\text{Pd}_{50}\text{Ag}_{50}$ and $\text{Pd}_{67}\text{Ag}_{33}$ for both the (111) and (100) plane at 800 K. The effect is more pronounced on the (100) plane, which is also observed by Rousset et al. [55]. The increase of surface segregation in the more open (100) surface compared to the (111) plane can be explained by the fact that surface energies are proportional to the number of broken bonds [72], [73]. Therefore, the difference between the surface energies of Ag and Pd is increased by the lower coordination number of the surface [57]. Furthermore, an oscillating segregation is seen for the $\text{Pd}_{25}\text{Ag}_{75}$ system on the (100) plane but not for the (111) plane. The 5th atomic layer is bulk like [3]. The computational methods of Rousset et al. [55] and Vurens et al. [70] report a similar oscillation.

The effect of a CO adsorption has been studied by Kuijers et al. using AES at 673 K at different compositions. Kuijers et al. report Ag segregation, the segregation is suppressed slightly when compared to the same system at the same temperature in a vacuum [63].

Table 1.1: Experimental surface segregation in Pd-Ag in vacuum for the (111) plane by various authors.

Ref.	Method	Temperature (K)	Composition bulk (at.%)	Composition surface (at.%)
Kuijers [63]	AES	673	$\text{Pd}_{67}\text{Ag}_{33}$	Ag segregates
Noordermeer [66]	AES, LEED	700	$\text{Pd}_{67}\text{Ag}_{33}$	$\text{Pd}_{5-10}\text{Ag}_{90-95}$
Wouda [68]	STM	720	$\text{Pd}_{67}\text{Ag}_{33}$	$\text{Pd}_5\text{Ag}_{95}$
		920	$\text{Pd}_{67}\text{Ag}_{33}$	$\text{Pd}_{11}\text{Ag}_{89}$

Table 1.2: Computational surface segregation in Pd-Ag in vacuum for the (111) plane by various authors.
*Modified mean-field model that includes subsurface layers.

Ref.	Method	Temperature (K)	Composition bulk (at.%)	Composition surface (at.%)
Zhao [69]	Miedema + LM	600	Pd ₇₅ Ag ₂₅	Pd ₄₈ Ag ₅₂
		820	Pd ₆₇ Ag ₃₃	Pd ₃₇ Ag ₆₃
Rousset [55]	Miedema/EAM + MC	800	Pd _x Ag _{100-x}	Ag segregates
Ropo [56]	DFT + Mean-field*	600	Pd ₇₀ Ag ₃₀	Pd ₁₂ Ag ₈₈
		900	Pd ₇₀ Ag ₃₀	Pd ₂₀ Ag ₈₀
		600	Pd ₅₀ Ag ₅₀	Pd ₁₀ Ag ₉₀
		900	Pd ₅₀ Ag ₅₀	Pd ₁₅ Ag ₈₅
		900	Pd ₃₀ Ag ₇₀	Pd ₃ Ag ₉₇
Ruban [57]	DFT + MC	800	Pd ₂₅ Ag ₇₅	Pd ₁ Ag ₉₉
			Pd ₆₇ Ag ₃₃	Pd ₁₂ Ag ₈₈
			Pd ₅₀ Ag ₅₀	Pd ₁₅ Ag ₈₅
Vurens [70]	Miedema + MC	870	Pd ₇₀ Ag ₃₀	Pd ₄₆ Ag ₅₄
Ropo [71]	DFT + LM	0	Pd ₅₀ Ag ₅₀	Pd ₀ Ag ₁₀₀
		300	Pd ₅₀ Ag ₅₀	Pd ₈ Ag ₉₂
		600	Pd ₅₀ Ag ₅₀	Pd ₁₉ Ag ₈₁
		900	Pd ₅₀ Ag ₅₀	Pd ₂₅ Ag ₇₅
		1200	Pd ₅₀ Ag ₅₀	Pd ₂₈ Ag ₇₂
Ouanasser [74]	TB-model + LM	1000	Pd ₇₅ Ag ₂₅	Pd ₁₀ Ag ₉₀
Foiles [75]	EAM + MC	1000	Pd ₅₀ Ag ₅₀	Pd ₂₄ Ag ₇₆

Surface segregation in Pd-Au

Table 1.3 shows the experimental results and table 1.4 shows the computational results reported in literature for Pd-Au. All authors report a surface segregation of Au and the experimental results agree with each other. Boes et al. [48] performed DFT calculations on Pd₅₀Au₅₀ and Yi et al. [67] performed experiments on the same composition and their results agree quantitatively. The computational results obtained by Boes et al. predict a segregation of 4 at.% Au larger than what Yi et al. find in experiments. Zhao et al. also performed calculations on the same composition and predict a segregation of 2 at.% Au larger than what Yi et al. find in experiments [76]. Another study by Zhao et al. studied surface segregation in Pd₇₅Au₂₅, their results are also in agreement with the results report by Yi et al. [69]. Zhao et al. [69], [76] and Creuze et al. [77] use the LM equation to compute the surface segregation which neglects SRO and their results agree quantitatively with computational and experimental results. Therefore, the effect of SRO seems to be negligible when determining the surface composition for Pd-Au at temperatures of 600 K and above. At temperatures below 700 K, experimental determinations of the equilibrium surface composition are hampered due to kinetic limitations of diffusion [48].

An oscillating enrichment of Au followed by a second atomic layer enriched in Pd is reported by Rousset et al. [55] and Boes et al. [48] using computational models. Yi et al. confirm an enrichment in the second atomic layer using XPS. Foiles reports a near bulk composition for the second atomic layer at 800 K. Boes et al. conclude that the enrichment of the second atomic layer is the result of SRO, which favours Pd-Au interactions over Pd-Pd and Au-Au interactions [48]. However, these interactions are expected to be weak, as they do not have a significant impact on the surface composition.

Gao et al. performed experiments to observe the effect of a CO atmosphere on the segregation of the Pd-Au system and report that at CO pressures larger than 13.3 Pa, Pd segregation is greatly enhanced [78]. This is confirmed by the computational models of Zhao et al. and Soto-Verdugo et al. [69], [79]. Furthermore, the model of Zhao et al. report Pd segregation when Pd-Au adsorbs and/or absorbs hydrogen, and report Pd segregation when oxygen is adsorbed.

Table 1.3: Experimental surface segregation in Pd-Au in vacuum by various authors.

Ref.	Method	Temperature (K)	Composition bulk (at.%)	Composition surface (at.%)
Yi [67]	LEIS, XPS	800	Pd ₅₀ Au ₅₀	Pd ₁₈ Au ₈₂
			Pd ₂₅ Au ₇₅	Pd ₆ Au ₉₄
			Pd ₇₅ Au ₂₅	Pd ₃₅ Au ₆₅
Hetzendorf [80]	LEIS + XPS	773	Pd _x Au _{100-x}	Au segregates
Swartzfager [81]	LEIS	875	Pd ₄₀ Au ₆₀	Pd ₅ Au ₉₅
			Pd ₆₀ Au ₄₀	Pd ₃₀ Au ₇₀

Table 1.4: Computational surface segregation in Pd-Au in vacuum for the (111) plane by various authors.

Ref.	Method	Temperature (K)	Composition bulk (at.%)	Composition surface (at.%)
Zhao [69]	Miedema + LM	600	Pd ₇₅ Au ₂₅	Pd ₂₉ Au ₇₁
Boes [48]	DFT + MC	800	Pd ₅₀ Au ₅₀	Pd ₂₂ Au ₇₈
Rousset [55]	Miedema/EAM + MC	800	Pd _x Au _{100-x}	Au segregates
Foiles [75]	EAM + MC	800	Pd _x Au _{100-x}	Au segregates
Zhao [76]	Miedema + LM	800	Pd ₅₀ Au ₅₀	Pd ₂₀ Au ₈₀
Creuze [77]	DFT + LM	800	Pd _x Au _{100-x}	Au segregates

Surface segregation in Pd-Cu

The reported surface segregation obtained by experimental and computational methods is shown in table 1.5 and 1.6 respectively. In general no, or a small Cu segregation is observed. This is explained by the competition between two effects, the surface energy effect causes Cu to segregate, while the elastic energy causes Pd to segregate. Although pure Pd and Cu are fcc metals, a bcc region exists as shown in the Pd-Cu phase diagram in figure 1.5 [82].

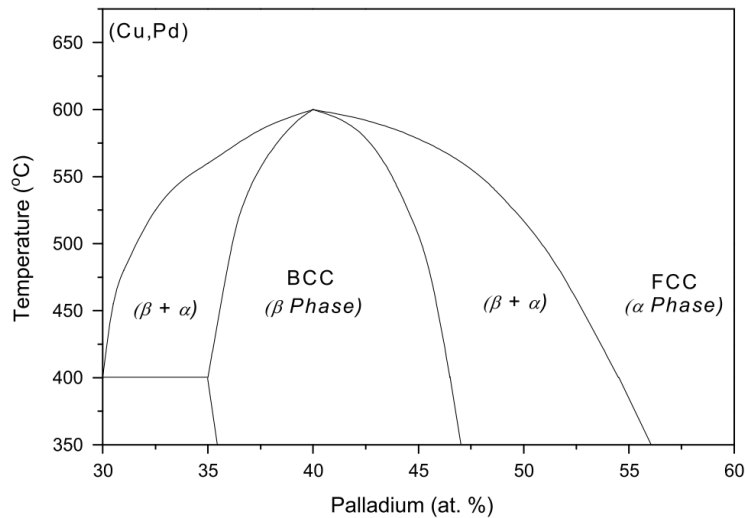


Figure 1.5: Pd-Cu phase diagram, showing a bcc region, from Nayebossadri et al. [82].

Rocherfort et al. and Noordermeer et al. report a small Cu segregation under vacuum, however their papers focus on the interaction between the alloy and a gas atmosphere and do not report the temperature at which their LEIS experiment were performed [83], [84]. Miller et al. show that the surface composition is dependent on the temperature at which the LEIS spectrum is obtained, which makes it difficult to draw any hard conclusions from the reported surface segregation from Rocherfort et al. and Noordermeer et al. [64]. Additionally, the composition used by Rocherfort et al. can be in the bcc phase, depending on the temperature, although Zhao et al. report that the difference in segregation between the fcc and bcc state is small [69]. Priyadarshini et al. performed high-throughput characterization on three different Pd-Cu alloys and report Cu segregation at all temperatures and compositions [85]. The computational results report no or a small Cu segregation, with the exception of the work from Vurens et al. which reports significant Cu segregation [70]. Vurens et al. shows that the accuracy of their results is limited due to the inaccuracy of the parameters that are used.

Cheng et al. performed kinetic MC simulations and verified their results against the experimental findings of Priyadarshini et al. and report good agreement [85], [86]. Substantial experimental research on Pd-Cu alloys has been devoted to the (110) plane, which shows Cu segregation [64], [87], [88]. Several authors report an oscillatory depth profile of a Cu-rich surface and a Pd-rich second layer on the (110) plane in vacuum [64], [87], [88].

Khanra et al. performed calculations on the (100) plane and report a Pd segregation for a hydrogen coverage of more than 0.75 monolayer [89]. Zhao et al. report a Pd segregation at 600 K with a monolayer hydrogen adsorbed. Pd segregation is also reported for 0.5 monolayer adsorbed and when hydrogen is adsorbed. An increasing oxygen adsorption results in an increase of Cu segregation. For a >0.25 monolayer CO adsorbed Pd will segregate, all computations are at 300 K at a composition of Pd₅₀Cu₅₀ [76]. The experimental result of Mousa et al. confirm a Pd segregation in a CO atmosphere for Pd₅₀Cu₅₀ at 550 K [90].

Table 1.5: Experimental surface segregation in Pd-Cu in vacuum for the (111) plane by various authors.

Ref.	Method	Temperature (K)	Composition bulk (at.%)	Composition surface (at.%)
Zhao [76]	LEIS, XPS	1000	Pd ₆₀ Cu ₄₀	Pd ₅₀ Cu ₅₀
Priyadarshini [85]	LEIS, XPS	700	Pd ₄₈ Cu ₅₂	Pd ₂₀ Cu ₈₀
		900	Pd ₄₈ Cu ₅₂	Pd ₂₄ Cu ₇₆
		700	Pd ₄₀ Cu ₆₀	Pd ₁₇ Cu ₈₃
		900	Pd ₄₀ Cu ₆₀	Pd ₁₉ Cu ₈₁
		-	Pd ₅₀ Cu ₅₀	Pd ₄₅ Cu ₅₅
Rocheftort [83]	LEIS, LEED, XPS	-	Pd ₅₀ Cu ₅₀	Pd ₄₅ Cu ₅₅
Noordermeer [84]	LEED, AES	-	Pd ₇₅ Cu ₂₅	Pd ₇₀ Cu ₃₀

Table 1.6: Computational surface segregation in Pd-Cu in vacuum for the (111) plane by various authors.

Ref.	Method	Temperature (K)	Composition bulk (at.%)	Composition surface (at.%)
Zhao [69]	Miedema + LM	600	Pd ₇₅ Cu ₂₅	Pd ₇₄ Cu ₂₆
Cheng [86]	Kinetic MC	700	Pd ₄₈ Cu ₅₂	Pd ₂₂ Cu ₇₈
		900	Pd ₄₈ Cu ₅₂	Pd ₂₃ Cu ₇₇
		700	Pd ₄₀ Cu ₆₀	Pd ₁₆ Cu ₈₄
		900	Pd ₄₀ Cu ₆₀	Pd ₁₈ Cu ₈₂
		800	Pd _x Cu _{100-x}	"near bulk"
Vurens [70]	Miedema + MC	870	Pd ₅₄ Cu ₄₆	Pd ₇₀ Cu ₃₀
Foiles [75]	EAM + MC	800	Pd _x Cu _{100-x}	"close to bulk"
Zhao [76]	Miedema + LM	1000	Pd ₆₀ Cu ₄₀	Pd ₅₂ Cu ₄₈
Gallis [91]	TB-model + LM	1400	Pd _x Cu _{100-x}	"segregation not very pronounced"

Surface segregation in Pd-Ni

Table 1.7 shows the experimental results and table 1.8 shows the computational results for surface segregation in Pd-Ni alloys. All authors report a strong Pd segregation to the surface. This can be explained by the strain energy induced by the larger size of Pd atoms compared to Ni atoms [92]. The computational results of Rousset et al. and Helfensteyn et al. agree quantitatively with the experiments and include the strain energy [55], [92]. Miegge et al. report a possible surface enrichment of Pd in the second layer. Rousset et al. report a Pd-enrichment of the first 3 layers when the bulk stays below 20 at.% Pd, when the bulk has more than 20 at.% Pd, Ni will start to segregate to the second layer. Derry et al. report an oscillating enrichment in Pd₅₀Ni₅₀ on the (100) surface using LEED. These results were confirmed by Helfensteyn et al and Poyurovskii et al. [92], [93]. Zhao et al. report a Pd segregation with hydrogen adsorption and Ni segregation with hydrogen absorption. When both hydrogen adsorption and absorption are considered, Ni will segregate [69].

Table 1.7: Experimental surface segregation in Pd-Ni in vacuum for the (111) plane by various authors.

Ref.	Method	Temperature (K)	Composition bulk (at.%)	Composition surface (at.%)
Michel [94]	LEIS, XPS	900	Pd ₈ Ni ₉₂	Pd ₇₆ Ni ₂₄
Miegge [95]	LEIS, XPS	870	Pd ₁ Ni ₉₉	Pd ₂₀ Ni ₈₀
			Pd ₅ Ni ₉₅	Pd ₅₀ Ni ₅₀

Table 1.8: Computational surface segregation in Pd-Ni in vacuum for the (111) plane by various authors.

Ref.	Method	Temperature (K)	Composition bulk (at.%)	Composition surface (at.%)
Zhao [69]	Miedema + LM	600	Pd ₇₅ Ni ₂₅	Pd ₉₇ Ni ₃
Rousset [55]	Miedema/EAM + MC	800	Pd _x Ni _{100-x}	Pd segregates
Helfensteyn [92]	EAM + MC	600 - 1000	Pd _x Ni _{100-x}	Pd segregates
Poyurovski [93]	EAM + MC	600	Pd ₅₀ Ni ₅₀	Pd segregates

Conclusion on surface segregation in Pd-based binary alloys

Segregation in Pd-based binary alloys is well studied and different driving forces can play a dominant role. Among others, surface segregation is dependent on the gas environment, temperature, enthalpies of mixing, surface energy, size mismatch of the atoms and the entropy contribution. In general, the surface energy is the dominant driving force [60], [61]. An example of the different dominating effects is seen when comparing the Pd-Cu and Pd-Ni system. Cu and Ni have similar atomic sizes and are smaller than Pd. This size mismatch induces a strain term which would lead to Pd segregation, as is the case for the Pd-Ni system. In the Pd-Cu system, the size mismatch is however compensated by the surface energy, which causes a balancing and a small Cu segregation is reported on the (111) plane in vacuum. Additionally, Ag and Au are chemically very similar [96]. At the same compositions and temperature, literature consistently reports larger Ag segregation than Au. One possible explanation could be a difference in the amount of electrons occupying the d-band. If the occupation of electrons is higher for Ag than for Au, the binding energy between Ag-Pd will be lower than Au-Pd. The lower binding energy between Ag-Pd can explain the larger segregation seen for Ag [97].

1.4. Surface segregation in ternary alloys

Surface segregation in binary alloys has been studied extensively. This is not the case for ternary alloys, even if (or perhaps because) the compositional space is larger. Pd-Ag-Cu and Pd-Cu-Au membranes have seen considerable attention due to their H₂ separation capabilities, especially from sulfur contaminated mixtures [18], [98]. Composition spread alloy films aid in speeding up obtaining results experimentally, as has been showed by Yin et al. and with a similar process by Galipaud et al., although these experiments remain costly and time-intensive [99], [100]. An example of a composition spread alloy film as shown in figure 1.6.

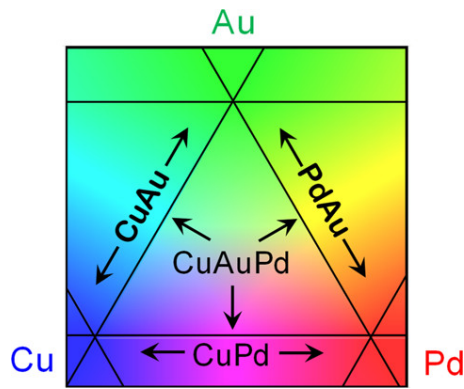


Figure 1.6: Representation of a composition spread alloy film, covering the entire composition range of a Pd-Cu-Au alloy from Yin et al. [99].

Surface segregation in Pd-Cu-Au

All constituents in the Pd-Cu-Au alloy are fcc, however a bcc region emerges upon mixing, as shown in figure 1.7 at 823 K, similar to the Pd-Cu alloy.

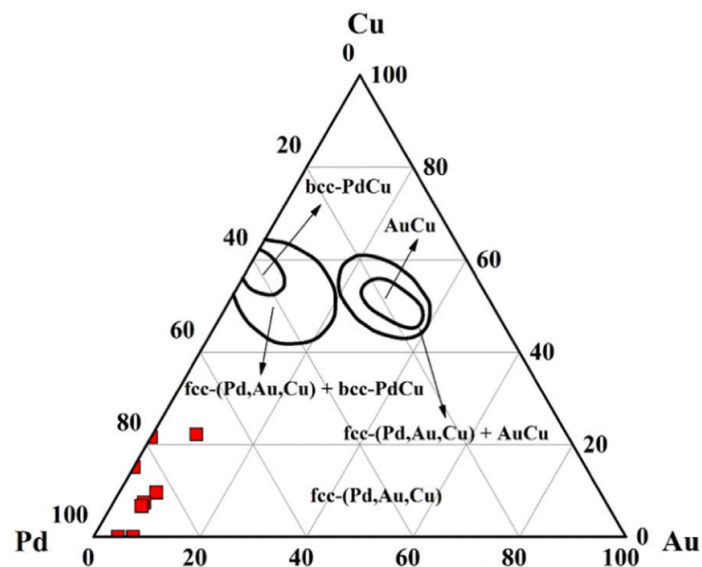


Figure 1.7: Phase diagram of Pd-Cu-Au at 823 K from Jia et al. [28].

Yin et al. performed surface segregation experiments on 164 different bulk compositions in the entire range of $\text{Pd}_{1-x-y}\text{Cu}_x\text{Au}_y$ using a composition spread alloy film. The bulk is measured by EDX and the surface under vacuum at 500 K and 600 K using LEIS [99]. From these experiments it is concluded that Au has the highest tendency to segregate, while Pd is always depleted from the surface. Higher temperatures lead to an enhanced segregation of Au. Cu segregates to the surface when the Au concentration is below approximately 20 at.%. Yin et al. compare their results against the three binary alloys contained in the ternary alloy (i.e. Cu-Au, Au-Pd and Pd-Au) as the composition spread alloy film is truly spanning the entire $\text{Pd}_{1-x-y}\text{Cu}_x\text{Au}_y$ range. For Pd-Au, Yin et al. report a Au segregation which is in agreement with the literature reported in the previous section. For Pd-Cu the results were similar to the work of Priyadarshini's [85]. However, the work of Yi et al. reports a bulk like composition at the surface around a $\text{Pd}_{50}\text{Cu}_{50}$ composition, which is not reported by Priyadarshini et al. It is argued that this is the result of the very fast cooling using liquid nitrogen which can freeze the PdCu into the high-temperature fcc phase [88]. Furthermore, Yin et al. conclude that segregation suppression exists in ordered phases in the bulk as a result of an enthalpy penalty. This penalty is the result of a disorder in the bulk, which forms when atoms segregate to the surface. Several experiments have been

performed on the Pd-Cu-Au system in non-vacuum environments. Tarditi et al. performed hydrogen permeation and composition experiments on Pd₇₁Cu₂₆Au₃ in the presence of H₂S [101] and report a Pd enrichment in approximately the top 10 nm of the specimen in a pure hydrogen environment. Below the near-surface region the composition was measured using XPS and was bulk like. After H₂S exposure the first 10 nm was enriched in S, the surface had a maximum atomic concentration of 15 at.% S. The Pd concentration decreased by approximately the same amount, suggesting that S replaced Pd in the near-surface region. Another study by Tarditi et al. compared 5 different Pd-Cu-Au alloys with a maximum Au fraction of 0.09 and studied the effect on the surface composition after S uptake [102]. Under a hydrogen atmosphere a Pd depletion is reported in the topmost layer and an enrichment in Cu using LEIS for all samples. The near-surface region (top 6 atomic layers) are enriched in Pd, which was measured using XPS and is in agreement with their other study [102]. The authors argue that Cu from the 2nd layer migrates to the surface layer, leading to a depletion of Pd in the surface layer, as this behaviour has been seen in Pd₇₀Cu₃₀ by Miller et al. [64].

Surface segregation in Pd-Cu-Ag

The Pd-Ag-Cu system is only in a single fcc phase when Cu is below 40 at. % at 773 K [47]. Zhao et al. report on a Pd_{60.6}Cu_{30.3}Ag_{9.1} sample, measured by EDS and study the surface segregation using XPS and LEIS. Furthermore, an extension of Miedema's model in combination with the LM equation is applied to predict surface segregation in ternary alloys. The results of Zhao et al. using Miedema's model in combination with the LM equation reported earlier are shown in table 1.9. As the two alloys annealed at 800 K were not yet in an equilibrium condition, these will not be considered. Additionally, the model considers a single crystal surface, which can result in a <3 at.% deviation. Quantitatively the model predicts co-segregation of Cu and Ag correctly. The Ag segregation is qualitatively predicted correctly, while the Cu segregation is predicted to be higher than what experiments show. By considering the three separate binary alloys (Pd-Cu, Pd-Ag, Ag-Cu), Zhao et al. discuss the co-segregation of Cu and Ag. Ag has a lower surface energy and lower mixing enthalpy with Pd than Cu, both increase the surface segregation of an element. Furthermore, Pd and Ag have a similar size and elastic moduli, therefore the much larger elastic strain energy is the driving force of the Cu atoms to the surface instead of Pd.

In a hydrogen environment, Zhao et al. performed LEIS where a strong Pd segregation is observed [103]. The LEIS experiments agree with the experiments performed by Tarditi et al. [18], [104]. A hydrogen atmosphere reverses the surface segregation behaviour of Cu and Ag, when compared to a vacuum and the surface is enriched in Pd.

Table 1.9: Reported segregation of Pd-Ag-Cu by Zhao et al. of the surface layer measured with LEIS and calculated using Miedema's model in combination with the LM equation [103].

Condition	Experimental Composition (at.%)		Calculated Composition (at.%)	
	Cu	Ag	Cu	Ag
Before segregation	29.4	10.4	30.0	10.0
1000 K in vacuum	45.1	15.3	54.4	16.5
1000 K in 1 bar H ₂	23.2	7.6	29.9	3.9

Tarditi et al. studied the Pd-Ag-Cu alloy which was annealed at 773 K for 120 h in a hydrogen atmosphere and report a surface enrichment of Pd and/or Ag using LEIS. Angle Resolved XPS in the same study confirms these results which concluded that the surface is depleted in Cu. No significant change of Pd was observed in the near-surface region. At higher temperatures a higher segregation of Ag surface is observed while the Cu concentration decreases. The co-segregation of Ag and Cu to the near-surface region is different from the observations made on the Pd-Cu-Au system by Tarditi et al., where a segregation of Pd is reported [101], [102]. The authors argue that this is due to the different

interaction of the minority component (i.e. Ag in the Pd-Ag-Cu system and Au in the Pd-Cu-Au system). Another study by Tarditi et al. confirmed a co-segregation of Ag and Cu in Pd₇₅Cu₂₁Ag₃, the near-surface region is measured using XPS after hydrogen permeation experiments for over 200 h at 593 - 693 K [104]. The Ag segregation is more pronounced at larger XPS angles (i.e. closer to the surface) while a decrease of Cu is seen. Furthermore, no significant Pd enrichment or depletion was seen in the near-surface region compared to the bulk.

Surface segregation in other ternary Pd-based alloys

In addition to the Pd-Ag-Cu alloy, Zhao et al. studied the Pd-Cu-Mo alloy, the surface layer is measured using LEIS and the bulk compositions are measured with EDS. Table 1.10 shows the reported experimental and computational segregation from Zhao et al. [103]. The calculations predict a surface completely depleted of Cu and Mo. However, the experimental results show that the Cu fraction stays almost the same while Mo is depleted. Mo has a strong tendency to stay in the bulk due to its larger surface energy [103]. Zhao et al. argue that the predicted Cu depletion in the computational model could be the result of the large negative mixing enthalpy of Cu with Mo. The effect of the hydrogen atmosphere and adsorption is small, this leads to a Pd segregation, similar to what is observed in vacuum.

Table 1.10: Reported segregation of Pd-Cu-Mo by Zhao et al. of the surface layer measured with LEIS and calculated using Miedema's model in combination with the LM equation [103].

Condition	Experimental Composition (at.%)		Calculated Composition (at.%)	
	Cu	Mo	Cu	Mo
Before segregation	5.2	10.9	5	10
1000 K in vacuum	6.0	3.6	0	0
1000 K in 1 bar H ₂	5.2	4.5	0	0

Yu et al. studied surface segregation in Pt-Pd-Rh using MEAM in combination with MC simulations in vacuum [105] and report a Pd enrichment on the (111) surface as a result of the lower surface energy of Pd. Due to the lack of experimental data on Pt-Pd-Rh, the authors compare their computational model against other ternary alloys and find qualitative agreement with the Cu-Ni-Au and Cu-Au-Ag systems. Luyten et al. also used MEAM in combination with MC to predict surface segregation in Pt-Pd-Rh on the (111) plane [106]. Luyten et al. report a Pd enrichment at 1200K for all bulk compositions. For a composition of Pt₄₀Pd₁₀Rh₅₀ on the (111) surface above 900 K a co-segregation of Pd and Rh is observed and below 900 K only Pd segregates to the surface. Aspera et al. performed DFT calculations

on the Pd-Ru-Rh system and report a Pd segregation [107]. Due to the lack of experimental data for the Pd-Ru-Rh system no validation of the model was made. Tafen et al. present a theoretical (DFT) and experimental (SEM, XPS) study on the Cu-Pd-Y ternary alloy which could function as a suitable membrane for the production of high purity hydrogen from syngas [108]. Using DFT in vacuum a segregation of Cu on the (011) plane is reported and an enrichment of Y in the 2nd atomic layer is reported. In an oxygen atmosphere, Y will segregate to the surface due to its larger oxygen affinity compared to Cu and Pd.

Conclusion on surface segregation in Pd-based ternary alloys

Literature on surface segregation in Pd-based ternary alloys is not reported as systematically as that for binary alloys. Furthermore, multi-body interactions arise in ternary alloys. The solute elements can interact by either attracting or repelling each other by different processes, such as, co-segregation, site-competition and blocking making it a more complex system [106]. Pd-Cu-Au and Pd-Cu-Ag behave similarly under vacuum conditions. Au and Ag segregate to the surface in their respective systems. In a hydrogen atmosphere a co-segregation of Ag and Cu to the near-surface region in Pd-Cu-Ag differs

from the observations made on the Pd-Cu-Au system by Tarditi et al., where a segregation of Pd is seen [101], [102]. It can be argued that this is the result of the different interaction of the minority component, which is Ag in the Pd-Ag-Cu system and Au in the Pd-Cu-Au system. The computational results from Zhao et al. which uses Miedema's model in combination with the LM equation on the Pd-Ag-Cu agree quantitatively with experiments, those on the Pd-Cu-Mo do not however. For both systems Zhao et al. report that the difference between computational and experimental results could in part be attributed to the assumption of an ideal solid solution. Miedema's model in combination with the LM equation is thus not able to qualitatively predict surface segregation on all ternary alloys. Validation of the few computational models on surface segregation in Pd-based ternary alloys that have been performed is difficult due to the lack of experimental data.

1.5. Research purpose

Literature on surface segregation in ternary alloys is limited. New methods are developed to obtain experimental data of surface segregation in ternary alloys at a faster rate and at a lower cost, such as composition spread alloy films [99], [100]. However, these experiments remain expensive and time-consuming. The combination of parameterizing Miedema's model to construct pairwise interactions between nearest-neighbours which can be used in MC simulations has not been performed before. This method can yield cheap and relatively fast screening of single-phase binary and ternary alloys and could yield quantitative results.

Research question

The main research question below has been constructed in order to fill the knowledge gap outlined above.

Are calculations using Miedema's model in combination with MC sufficiently fast and reliable to predict and screen surface segregation in ternary alloys?

To answer this question, two sub-questions have to be answered.

1. *How reliably can Miedema's model predict the segregation enthalpy of ternary alloys when only pairwise interactions from nearest-neighbors are considered?*
2. *How large is the effect of deviating from a perfectly random solid solution by using Monte Carlo simulations instead of the LM equation on the predicted surface segregation?*

Scope

A scope has been set up in order to list the goals and objectives of this work. Within the scope of the project fall:

- Writing a computational model that uses Miedema's model and MC simulations in Python to predict surface segregation in binary and ternary alloys in a vacuum and gas atmospheres.
- The computational model will be restricted to surface segregation of fcc systems on the (111) plane.
- Validating the results against currently available experimental and computational literature.
- The binary and ternary alloys will contain at least one transition metal.

Outside of the scope of the project fall:

- Absorption of gasses from the atmosphere and their effect.
- Experimental verification of the computational model.

2

Methodology

The methodology outlines the theory of the computational framework to model surface segregation in ternary alloys in both a vacuum and a gas environment. The methodology starts off with a background, which describes Monte Carlo simulations and Miedema's model in more detail, which form the basis on which the computational model is build. First the behaviour of atomic movement of a binary alloy in bulk is described and is used to then model a slab with two surfaces in a vacuum environment. This model is then extended to a binary alloy in a gas environment and finally to describe surface segregation in ternary alloys in both a vacuum and a gas environment.

2.1. Miedema's model for mixing enthalpy

Miedema's model has been successfully applied to calculate the mixing enthalpy of binary alloys [103], [109]. Miedema's model uses the energy changes that arise when individual atoms are embedded in an alloy. Two energy effects arise, the first one is due to the discontinuity between the density of electrons at the boundary of the Wigner-Seitz atomic cell n_{ws} which has to be smoothed. The smoothing of the difference in electron-density results in a volume change of the atomic cells in the alloy compared to their original equilibrium volumes. Therefore, a change in volume will lead to a positive contribution to the alloying energy. The second energy effect is due to the difference in the chemical potential ϕ^* . Due to the preference of electrons to be at a lower potential energy, the charge will be redistributed, resulting in a lower energy of the alloy [109], [110]. Additionally, a contraction parameter a , and three proportionality parameters P , Q and R , which are determined on the basis of experimental data are used. Various alterations have been made in order to extend Miedema's model to ternary alloys, with varying success. The general approach for extending the Miedema's model to ternary alloys is by using the sub-binary alloys that are contained in the ternary alloy [50], [103], [111]–[116]. The extended Miedema's model by Zhao et al. to calculate surface segregation energies, is a combination of two variations of Miedema's model and includes the configurational energy and elastic strain energy and is used in this work [103].

Miedema's model is a semi-empirical model that can be used for estimating the heats of formation $H_{AinB}^{formation}$. An accuracy of about 30% is achieved if metals with predominant s and d character in their conduction-electron states are considered [110]. The alloy parameter ω describes which type of bonds are preferred, if $\omega > 0$ bonding between the same type of atoms is preferred and if $\omega < 0$, bonds between dislike atoms are preferred. Therefore, it plays a key role in the surface segregation. The alloy parameter is directly related to the mixing enthalpy ΔH_{mix} . For a binary alloy that is in a regular solid solution, ω is defined as

$$\omega = \frac{\Delta H_{mix}}{\chi_A(1 - \chi_A)} \quad (2.1)$$

Where χ_A is the concentration of the solute expressed in atomic fraction [117]. In Miedema's model the mixing enthalpy is assumed to be equal to the formation enthalpy and can be computed with

$$\Delta H_{mix} = H_{AinB}^{formation} = c_A^S f_B^A \Delta H_{AinB}^{sol} \quad (2.2)$$

H_{AinB}^{sol} represents the formation enthalpy and is evaluated by

$$\Delta H_{AinB}^{sol} = \frac{(V_A^{2/3})_{alloy}}{(n_{ws}^{-1/3})_{avg}} [-P(\Delta\phi^*)^2 + Q(\Delta n_{ws}^{1/3})^2] \quad (2.3)$$

Where V_A and V_B represent the molar volume of element A and B respectively, $P = 12.35$, $Q = 115.62$ and $R = 47.97$ are empirical constants and n_{ws} represents the electron density at the boundary of the Wigner-Seitz atomic cell where

$$\Delta(n_{ws}^{-1/3})_{avg} = n_{wsA}^{1/3} - n_{wsB}^{1/3} \quad (2.4)$$

and

$$(n_{ws}^{-1/3})_{avg} = \frac{n_{wsA}^{-1/3} - n_{wsB}^{-1/3}}{2} \quad (2.5)$$

and ϕ^* the chemical potential for electronic charge where

$$\Delta\phi^* = \phi_A^* - \phi_B^* \quad (2.6)$$

Furthermore, c_A is the atomic solute fraction and f_B^A is a parameter representing the degree to which an atomic cell of A is surrounded by B (i.e. $f_B^A = 1$, A fully surrounded by B). f_B^A has no further physical significance and is computed with equation 2.7. According to Miedema et al., it is the simplest analytical function to approximate the concentration dependence of the heat of formation[110].

$$f_B^A = (1 - c_A^S)[1 + 8(c_A^S)^2(1 - c_A^S)^2] \quad (2.7)$$

Where c_A^S represents the surface fraction of A atoms in B and is related to the molar volume V_A and V_B respectively. It is important to note that the value for c_A^S is not the same as the final surface concentration. c_A^S is computed as

$$c_A^S = \frac{c_A(V_A^{2/3})_{alloy}}{c_A(V_A^{2/3})_{alloy} + c_B(V_B^{2/3})_{alloy}} \quad (2.8)$$

The alloyed volume is computed as

$$\frac{(V_A^{2/3})_{alloy}}{(V_A^{2/3})_{pure}} = 1 + \alpha f_B^A (\phi_A^* - \phi_B^*) \quad (2.9)$$

Where $\alpha = 0.04$ and equation 2.7, 2.8 and 2.9 need to be solved in a self consistent manner.

2.2. Monte Carlo simulations

MC simulations are used in various fields and rely on random sampling. In materials science they can yield thermodynamic information about a system. Typical MC simulations used in statistical mechanics consider a system with a constant temperature, constant number of particles and a constant volume. Atoms are switched until the energy of the system no longer decreases apart from random thermal fluctuations. At this point thermodynamical equilibrium is reached. This thermodynamical equilibrium is however not unique. Above 0 K the entropy is non-zero and this term allows certain atomic movements that increase the energy to take place. Therefore, the statistical ensemble is considered, which is an average of various micro-states to get a representative macro state of the system. Periodic boundary conditions are considered. The system should follow the detailed balance which states that each atomic switch is in equilibrium with its reverse process.

In a vacuum the segregation enthalpy is a function of the configurational enthalpy and the elastic energy. The configurational enthalpy computed by Miedema's model is parameterized, as will be showed in the following section. In the model from this work the simplest way possible to model the interactions

between atoms is chosen, that is only pairwise interactions between nearest-neighbors are considered. Using the Metropolis algorithm two atoms are randomly selected and it is determined whether this switch is favourable or not. The pseudo code shown in algorithm 1 shows the Metropolis algorithm used in the model. If switching two atoms results in an increase of the systems total energy, the state is kept only if the condition in equation 2.10 is true.

$$p < \exp\left(\frac{-\Delta H_{seg}}{k_B T}\right) \quad (2.10)$$

Where ΔH_{seg} is the energy associated to the switch and computed in the following section, k_B is the Boltzmann constant, T the temperature and p a random float between 0 and 1. In this work the temperature is linearly brought down from 2000 K to the final temperature over the first 5% of MC steps. This ensures that the system is able to overcome local minima in which the system could otherwise get stuck.

Algorithm 1 Metropolis Algorithm

```

for  $i = 1, i++,$  while  $i < n\_MC\_Steps$  do
  Pick random atom a1
  while True do
    Pick random atom a2
    if element a1  $\neq$  element a2 then
      break
    end if
  end while
   $\Delta H_{seg} =$  switch atom a1 and a2
  if  $\Delta H_{seg} < 0$  then
    Switch a1 and a2
  else
     $p =$  random integer between 0 and 1
    if  $p < \exp(-\Delta H_{seg}/k_B T)$  then
      Switch a1 and a2
    else
      keep current configuration
    end if
  end if
end for

```

2.3. Computational model for binary alloys

Configurational energy in bulk

Atomic switches are first considered only in the bulk and only nearest neighbour interactions are considered. Let an atom be in the bulk at site 1, it will have Z_1^A neighbors of type A and Z_2^A neighbors of type B. Then $Z = Z_1^A + Z_1^B$, where Z is the total amount of neighbors in the bulk, i.e. 12 in an fcc lattice. The energy associated to removing an A atom from site 1 and adding it to site 2 are given by

$$U_{remove}^A = -Z_1^A \cdot \varepsilon_{AA} - Z_1^B \cdot \varepsilon_{AB} \quad (2.11)$$

$$U_{add}^A = Z_2^A \cdot \varepsilon_{AA} + Z_2^B \cdot \varepsilon_{AB} \quad (2.12)$$

Similarly removing a B atom from site 2 and adding it to site 1 yields

$$U_{remove}^B = -Z_2^B \cdot \varepsilon_{BB} - Z_2^A \cdot \varepsilon_{AB} \quad (2.13)$$

$$U_{add}^B = Z_1^B \cdot \varepsilon_{BB} + Z_1^A \cdot \varepsilon_{AB} \quad (2.14)$$

Where ε_{AA} , ε_{BB} and ε_{AB} represent the binding energies between pairs of atoms. From which the total energy associated to the switch can be computed by:

$$\Delta E_{conf} = U_{remove}^A + U_{add}^A + U_{remove}^B + U_{add}^B \quad (2.15)$$

Using the following two substitutions:

$$\begin{aligned} Z_1^B &= (Z - Z_1^A) \\ Z_2^B &= (Z - Z_2^A) \end{aligned} \quad (2.16)$$

The total configurational energy is given by

$$\Delta E_{conf} = (-\varepsilon_{AA} - \varepsilon_{BB} + 2\varepsilon_{AB})(Z_1^A - Z_2^A) \quad (2.17)$$

Let ω be [60].

$$\omega = \varepsilon_{AB} - \frac{\varepsilon_{AA} + \varepsilon_{BB}}{2} \quad (2.18)$$

Substitution of equation 2.18 in equation 2.17 yields the configurational energy change of exchanging an A and a B atom in the bulk

$$\Delta E_{conf} = 2\omega(Z_1^A - Z_2^A) \quad (2.19)$$

Surface segregation

The method described in the paper by Zhao et al. is used to model surface segregation [69]. The segregation enthalpy in a vacuum depends on the elastic strain energy and the configurational energy change as shown in equation 2.20.

$$\Delta H_{seg} = \Delta E_{conf} + \Delta E_{elastic} \quad (2.20)$$

In a slab of a binary or ternary alloy three types of atomic switches can occur. In comparison to one configurational switch in bulk (i.e. bulk-bulk). These configurational changes are shown in figure 2.1.

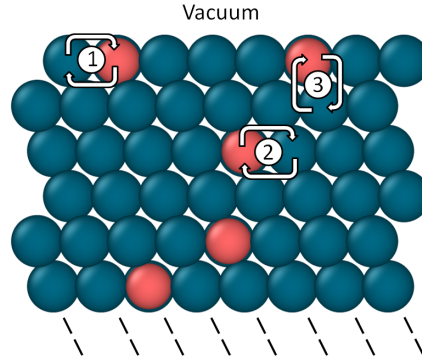


Figure 2.1: Possible atomic switches in a slab, the top is exposed to vacuum while the bottom continuing bulk. 1) surface-surface switch, 2) bulk-bulk switch and 3) bulk-surface switch.

Configurational enthalpy

The energy change of removing an A atom from the surface and adding that atom to the bulk is the same as described by equation 2.11 and equation 2.12 respectively. Similarly, removing a B atom from the bulk and adding it to the surface is described by equation 2.13 and equation 2.14. The total number of neighboring atoms on the surface differs to that of the bulk, the two substitutions from the aforementioned equations change to $Z_1^B = (Z_L + Z_V - Z_1^A)$ and $Z_2^B = (Z_L + Z_V - Z_2^A)$, where Z_L is the number of lateral atoms and Z_V the number of vertical atoms, which take the value of 6 and 3 respectively in an fcc lattice. If the atom considered in the bulk, the value of Z_V will thus change to $2Z_V$. Exchanging a bulk atom by a surface atom results in an energy change

$$\Delta E_{conf} = 2\omega(Z_1^A - Z_2^A) + Z_V(-\varepsilon_{AB} + \varepsilon_{BB}) \quad (2.21)$$

By calling $\varepsilon_{BB} = \frac{1}{2}\varepsilon_{BB} + \frac{1}{2}\varepsilon_{BB}$ and adding $\frac{1}{2}\varepsilon_{AA} - \frac{1}{2}\varepsilon_{AA}$ equation 2.21 can be rewritten to

$$\Delta E_{conf} = 2\omega(Z_1^A - Z_2^A) + Z_V\omega + Z_V\left(\frac{1}{2}\varepsilon_{BB} - \frac{1}{2}\varepsilon_{AA}\right) \quad (2.22)$$

Substituting $-\frac{Z_V \epsilon_{AA}}{2} = \gamma_A \sigma_A$ yields the surface energy contributions for A and B. Resulting in energy associated to exchanging an A atom in the bulk by a B atom on the surface described by

$$\Delta E_{conf} = 2\omega(Z_1^A - Z_2^A) + Z_V \omega + \gamma_A \sigma_A - \gamma_B \sigma_B \quad (2.23)$$

Where the value of ω is evaluated by Miedema's model.

Elastic energy

The elastic energy of an arbitrary element A in B is described by Friedel [118] and Abraham et al. [119] for very dilute binary solid alloys as

$$\Delta E_{elastic}^{AinB} = \frac{2K_A G_B (V_A - V_B)^2}{3K_A V_B + 4G_B V_A} \quad (2.24)$$

Where V is the atomic volume, K the bulk modulus and G the shear modulus. The subscript A corresponds to the solute and the subscript B corresponds to the solvent. As a result of the mean-field nature of the elastic energy term, it cannot be described by pairwise interactions, in contrast to the configurational energy term. This follows from the fact that the elastic energy is totally relaxed at the surface [119], therefore only a bulk-surface or surface-bulk switch results in a net energy change of the elastic energy. If the elastic energy was considered a pairwise interaction, the total energy would drift. A convincing way to support this is the following thought-experiment, shown in figure 2.2. If the

red atoms are very soft, no energy is released when they are brought to the surface. Additionally, for every blue atom that moves from the surface to the bulk, energy is released. Lets give this the arbitrary energy value of -1 eV per bond with a red atom that is gained. Similarly, for every blue atom that moves from the bulk to the surface, an energy of 1 eV per bond with a blue atom is gained. The top left figure shows an initial configuration where the top layer represents the surface layer. If atom A from the bulk is switched with atom B is on the surface, there is a relaxation energy of -8 eV. Since the B atom in the bulk gains 8 red atoms as neighbors, as shown in in 2.2b. If atoms C and D are now exchanged, the blue atom D loses 7 blue neighbors, which corresponds to + 7 eV. Then atom E and F are exchanged, which does not have an effect on the elastic energy/relaxation. At this point figure 2.2d and figure 2.2a are the same, however the net energy change is -1 eV. In other words, the local elastic energy caused by bulk-surface and surface-bulk switches are not balanced by bulk-bulk switches. Resulting in an energy drift and the detailed balance is broken, hence the elastic energy is used a mean field term.

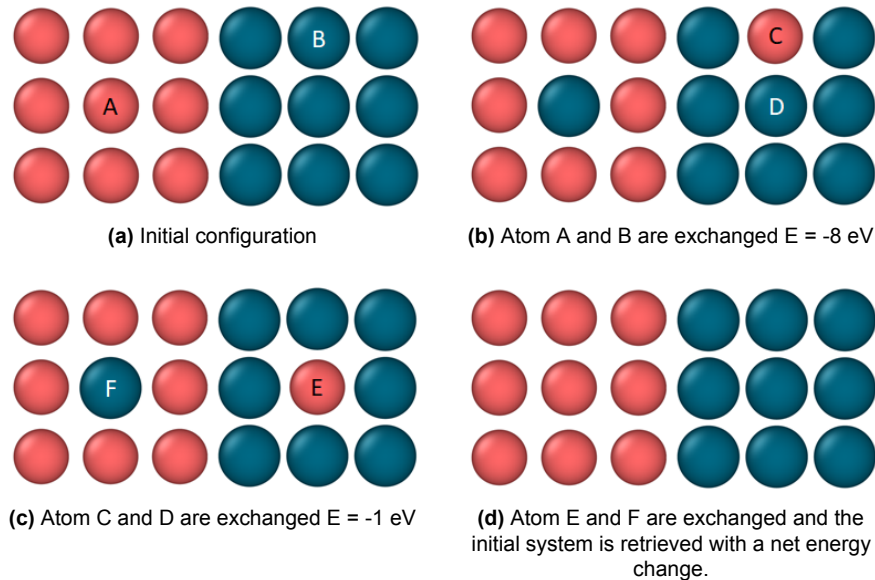


Figure 2.2: Example of elastic drift as a result of a pairwise elastic energy term.

The equation for the elastic energy as originally introduced in the dilute limit is non-symmetric. This results in artificially different values of the elastic energy at a 50/50 composition when the solute and

solvent are switched. The weighted average by composition can be taken of the elastic energy to solve this, resulting in equation 2.25 which is anti-symmetric.

$$\Delta E_{elastic} = E_{elastic}^{AinB} \cdot c_B - E_{elastic}^{BinA} \cdot c_A \quad (2.25)$$

Where c_A and c_B are the weight fraction of the solute and solvent respectively. It was found that this was not considered in the model proposed by Zhao et al. [69]. This results in a different segregation pattern when the solvent and solute are switched and can account for 10% difference in the predicted surface segregation in a 50:50 alloy.

Hydrogen adsorption

Hydrogen and other gases can adsorb to the surface and affect surface segregation. The adsorption enthalpy needs to be considered in order to describe the interaction between the alloy and the hydrogen environment. The segregation energy equation thus contains one more term as seen in equation 2.26.

$$\Delta H_{seg} = \Delta E_{conf} + \Delta E_{elastic} + \Delta H_{ads} \quad (2.26)$$

The adsorption enthalpy is a function of the chemical potential of hydrogen in the gas phase, which is a function of temperature, is considered ideal and is computed with

$$\mu(P, T) = \mu_0^i + RT \ln \left(\frac{P}{P_0} \right) \quad (2.27)$$

Where R is the gas constant, T the temperature, μ_0^i the standard chemical potential of a pure ideal gas, P the pressure and P_0 the reference pressure.

The hydrogen coverage is not fixed in this model and hydrogen atoms can adsorb and desorb from the surface using the metropolis algorithm. The hydrogen atoms preferentially adsorb on the fcc hollow sites [120]. Furthermore, the adsorption enthalpy is a function of the hydrogen adsorption energy. The hydrogen adsorption energies are taken from Wynblatt et al. and Tomanek et al. [29], [60]. The hydrogen atom when adsorbed on an fcc site is surrounded by three atoms as shown in figure 2.3. The average adsorption energy of the three atoms surrounding the hydrogen atom is taken as the hydrogen adsorption energy of that position. The approach for hydrogen adsorption and desorption shown in the pseudo code of algorithm 2. Thus the adsorption energy is evaluated as

$$\Delta H_{ads} = E_{ads} - \mu(P, T) \quad (2.28)$$

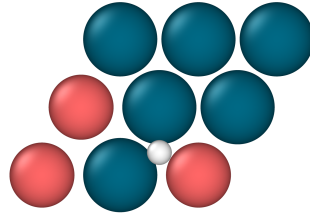


Figure 2.3: Position of one hydrogen atom (white) adsorbed on a fcc position, surrounded by two blue atoms and one red atom.

Algorithm 2 Hydrogen adsorption

```

for  $i = 1, i++,$  while  $i < n\_MC\_Steps$  do
   $p = \text{random integer between 0 and 1}$ 
  if  $p < 0.01$  then
     $ph = \text{random integer between 0 and 1}$ 
    Pick random fcc position on the surface
    Find atoms surrounding fcc position
    if fcc position empty then
      if adsorption lowers energy then
        Add hydrogen atom
      else
        if  $ph < \exp(-\Delta H_{ads}/k_B T)$  then
          Add hydrogen atom
        else
          keep current configuration
        end if
      end if
    end if
  else
    if removing hydrogen reduces energy then
      Remove hydrogen atom
    else
      if  $ph < \exp(-\Delta H_{ads}/k_B T)$  then
        Remove hydrogen atom
      else
        keep current configuration
      end if
    end if
  end if
end if
end if
end for

```

For hydrogen adsorption energies which are not described in literature, DFT is used to compute these values and is further explained in section 2.5. Hydrogen interacting with other hydrogen atoms on the surface plays a role at temperatures below 200 K and can result in different forms of ordering of the hydrogen atoms [121]. These hydrogen interactions are neglected as the model will compute surface segregation at temperatures that exceed 200 K.

2.4. Computational model for ternary alloys

Similar to the work of Zhao et al. a combination of the geometric Miedema's model by Ouyang et al. [103], [113] and a two-step Miedema's model by Wang et al. is used [114]. First the behaviour in a ternary bulk alloy will be described.

Bulk

The same method to derive the energy associated to switching two atoms in the bulk for ternary alloys is used as the method that was used for binary alloys. This yields

$$U_{remove}^A = -Z_1^A \cdot \varepsilon_{AA} - Z_1^B \cdot \varepsilon_{AB} - Z_1^C \cdot \varepsilon_{AC} \quad (2.29)$$

$$U_{add}^A = Z_2^A \cdot \varepsilon_{AA} + Z_2^B \cdot \varepsilon_{AB} + Z_2^C \cdot \varepsilon_{AC} \quad (2.30)$$

Similarly removing a B atom from site 2 and adding it to site 1 is described by

$$U_{remove}^B = -Z_1^B \cdot \varepsilon_{BB} - Z_1^A \cdot \varepsilon_{AB} - Z_1^C \cdot \varepsilon_{BC} \quad (2.31)$$

$$U_{add}^B = Z_2^B \cdot \varepsilon_{BB} + Z_2^A \cdot \varepsilon_{AB} + Z_2^C \cdot \varepsilon_{BC} \quad (2.32)$$

The total energy change of switching these two atoms in the bulk is computed by summing these four equations

$$\Delta E_{conf} = U_{remove}^A + U_{add}^A + U_{remove}^B + U_{add}^B \quad (2.33)$$

Applying the following two substitutions

$$\begin{aligned} Z_1^C &= (Z - Z_1^A - Z_1^B) \\ Z_2^C &= (Z - Z_2^A - Z_2^B) \end{aligned} \quad (2.34)$$

and with the three alloying parameters

$$\begin{aligned} \omega_{AB} &= \varepsilon_{AB} - \frac{\varepsilon_{AA} + \varepsilon_{BB}}{2} \\ \omega_{AC} &= \varepsilon_{AC} - \frac{\varepsilon_{AA} + \varepsilon_{CC}}{2} \\ \omega_{BC} &= \varepsilon_{BC} - \frac{\varepsilon_{BB} + \varepsilon_{CC}}{2} \end{aligned} \quad (2.35)$$

The configurational energy change in the bulk when switching atom A and B is

$$E_{conf} = (Z_1^A - Z_2^A)(\omega_{AB} + \omega_{AC} - \omega_{BC}) + (Z_1^B - Z_2^B)(-\omega_{AB} + \omega_{AC} - \omega_{BC}) \quad (2.36)$$

Surface Segregation

The equation for the segregation enthalpy from binary alloys, equation 2.20, also holds for ternary alloys and is repeated below.

$$\Delta H_{seg} = \Delta E_{conf} + \Delta E_{elastic}$$

The configurational and elastic energy are however derived in a different fashion to account for the third element, and are presented in the following sections. The hydrogen adsorption enthalpy is computed similarly to what was presented in binary alloys and is therefore not covered again.

Miedema's model for mixing enthalpy in ternary alloys

The values of ω depend on the mixing enthalpy (equation 2.1, repeated below).

$$\omega_{AB} = \frac{\Delta H_{AB}^{mix}}{Z\chi_A\chi_B}$$

The mixing enthalpy is computed with Miedema's model, which is derived differently than that of binary alloys to account for the third element. Wang et al. first propose a correction factor for the solution enthalpy which yields a lower average error compared to the experimental values. This correction factor is

$$S(\chi) = 1 - \frac{\chi_A\chi_B|V_A - V_B|}{2(\chi_A\chi_A V_A + \chi_B\chi_B V_B)} \quad (2.37)$$

Where χ_A and χ_B are the bulk concentrations expressed in atomic fraction and V_A and V_B the molar volume of element A and B respectively. This results in a new equation for the solution enthalpy namely

$$\Delta H_{AinB}^{sol} = \frac{S(\chi)(V_A^{2/3})_{alloy}}{(n_{ws}^{-1/3})_{avg}} [-P(\Delta\phi^*)^2 + Q(\Delta n_{ws}^{1/3})^2] \quad (2.38)$$

The reader is referred to section 2.3 for a reminder of the meaning of these parameters and the following parameters. Wang et al. propose a two-step Miedema's model where the mixing enthalpy of the sub-binary alloy A-B is computed. This alloy AB is then considered as a new alloy and the new mixing enthalpy is computed for the pseudobinary AB-C alloy, which yields [114].

$$\Delta H_{AB}^{mix} = \frac{1}{3}(\Delta H_{AinB} + \Delta H_{CinAB}) \quad (2.39)$$

$$\Delta H_{CinAB} = (\chi_A + \chi_B)\chi_C(f_{AB}^C \Delta H_{CinAB}^{sol} + f_C^{AB} \Delta H_{ABinC}^{sol}) \quad (2.40)$$

$$\Delta H_{AB} = (\chi_A + \chi_B)(f_A^B \Delta H_{AinB}^{sol} + f_B^A \Delta H_{BinA}^{sol}) \quad (2.41)$$

Configurational Enthalpy

Equations 2.29 to 2.35 from the bulk are used to compute the configurational enthalpy related to surface segregation. To account for the surface atoms the two substitutions have to be replaced by the equations shown below. If an atom is in the bulk the value will have to be changed to $2Z_V$.

$$\begin{aligned} Z_1^C &= (Z_L + Z_V - Z_1^A - Z_1^B) \\ Z_2^C &= (Z_L + Z_V - Z_2^A - Z_2^B) \end{aligned} \quad (2.42)$$

Furthermore, substituting $-\frac{Z_V \epsilon_{AA}}{2} = \gamma_A \sigma_A$ yields the surface energy contributions for A and B. The configurational enthalpy of exchanging a surface atom A by a bulk atom B can be evaluated by

$$\begin{aligned} \Delta E_{conf} &= (Z_1^A - Z_2^A)(\omega_{AB} + \omega_{AC} - \omega_{BC}) + (Z_1^B - Z_2^B)(-\omega_{AB} + \omega_{AC} - \omega_{BC}) \\ &\quad + Z_v \omega_{BC} - Z_v \omega_{AC} + \gamma_A \sigma_A - \gamma_B \sigma_B \end{aligned} \quad (2.43)$$

Elastic Energy

The equation for the elastic energy presented in the binary alloys section, equation 2.24, cannot directly be used for ternary alloys as the third element has to be taken into account. Several methods exist to convert the elastic energy from a binary alloy to a ternary alloy, many of which are asymmetrical and require user input. To overcome these asymmetrical models, Chou et al. propose that rather than fixing the composition of the three binary alloys contained in the ternary alloy, the compositions should always be related to the three components themselves [122]. This model presented by Chou et al. is applied by Ouyang et al. which is in turn applied by Zhao et al. which forms the basis of the model presented in this work [103], [113]. The elastic strain energy in ternary alloys is thus evaluated using the geometric model as proposed by Ouyang et al. and computed with equation 2.44 [113].

$$\Delta E_{elastic}^{AB}(\gamma_{AB}^A, \gamma_{AB}^B) = \gamma_A \gamma_B (\gamma_B \Delta E_{elastic}^{AinB} + \gamma_A \Delta E_{elastic}^{BinA}) \quad (2.44)$$

where $E_{elastic}^{AinB}$ is the elastic energy of element A in B, and,

$$\gamma_{AB}^A = \chi_C + \delta_{AB}^A \chi_C, \quad \gamma_{AB}^B = \chi_B + \delta_{AB}^B \chi_C \quad (2.45)$$

with

$$\delta_{AB}^A = \frac{\lambda_A}{\lambda_A + \lambda_B}, \quad \delta_{AB}^B = \frac{\lambda_B}{\lambda_A + \lambda_B} \quad (2.46)$$

and

$$\lambda_A = (\Delta H_{BinA}^{sol} - \Delta H_{CinA}^{sol})^2 \quad (2.47)$$

where the reader is referred to section 2.3 for the computation of the solution enthalpies. Similarly to binary alloys, to preserve the detailed balance the elastic energy is computed as

$$E_{elastic} = \Delta E_{elastic}^{AinB} \cdot c_A - \Delta E_{elastic}^{BinA} \cdot c_B + c_C \cdot (\Delta E_{elastic}^{CinB} - \Delta E_{elastic}^{CinA}) \quad (2.48)$$

when switching an A atom from the surface to a B atom in the bulk.

2.5. Density functional theory for hydrogen adsorption energies

The hydrogen adsorption energy can have a large effect on the type of element that will surface segregate. Therefore the hydrogen adsorption energy has to be known for each element that is being screened. The hydrogen adsorption energy has been reported for various elements. For the hydrogen adsorption energy on elements that are unknown, DFT calculations are performed. This is done by computing the energy associated to a H_2 molecule, that of a metal slab and that of a metal slab with hydrogen atom adsorbed on either side. Using these energies the hydrogen adsorption energy can be computed as

$$\Delta H_{ads} = \frac{E_{M+2H} - E_M - E_{H_2}}{2} \quad (2.49)$$

Where E_{M+2H} is the energy of the metal in combination with a hydrogen atom adsorbed on both sides of the slab, E_M is the energy associated to the metal slab in vacuum and E_{H_2} the energy of a

hydrogen molecule. These computations were performed using the plane-wave projector augmented wave (PAW) as implemented in VASP 5.4 [123]–[125]. The generalized gradient approximation in the PBE parametrization was used for the PAW method [126]. The energy cutoff was varied from 300 eV to 500 eV. Smearing of the electronic states was applied with the tetrahedron method. The fcc(111) surfaces are modeled as a 1 x 1 x 7 slab with 30 Å of vacuum. The surfaces with hydrogen adsorbed on either side use the same structure with one hydrogen atom adsorbed on either side of the slab on the fcc hollow site. For the slabs the k-mesh is varied between 20 x 20 x 1 and 25 x 25 x 1 and for the hydrogen molecule a k-mesh of 2 x 2 x 2 is used. The atomic positions are relaxed until the energy decreased by less than 10^{-4} eV. A maximum difference of 0.05 eV/atom is found when converging from an energy cutoff of 300eV to 500 eV. The results are compared to existing literature in table 2.1, the complete list is shown in Appendix A. For Ni a difference of 0.17 eV/atom is seen between the experimental results of Tomanek et al. and those from Watson et al. using DFT [29], [120]. The results obtained from DFT in this work match those of Watson et al. for both Ni and Pd. However, a difference of 0.35 eV/atom is seen in Ag. For consistency the results of Tomanek et al. will be used where possible, otherwise the hydrogen adsorption energies computed with DFT from this work will be used.

Table 2.1: Hydrogen adsorption energies computed with DFT and compared against literature.

Element	E_{ads} (eV/atom)		Source
	Literature	This work	
Ag	-0.11	0.24	[29]
Ni	-0.48	-0.63	[29]
	-0.65		[120]
Pd	-0.48	-0.49	[29]
	-0.48		[127]
	-0.50		[120]

2.6. Thermo-Calc for calculation of phase diagrams

Phase diagrams can provide insight on the equilibrium structure of an alloy as a function of temperature and pressure. Thermo-Calc is a software package that can be used for the calculation of phase diagrams (CALPHAD) of ternary alloys [128]. It uses data on phase equilibria, crystal structure and thermochemical data in combination with free parameters to construct the phase diagrams of ternary alloys. In the current work, Thermo-Calc is used to screen through a wide range of ternary alloys at various temperatures and pressures to find the compositional ranges in which a single fcc phase is stable.

3

Verification against literature

This chapter will compare experimental and computational surface segregation presented in Chapter 1 against the results that are obtained by the computational model from this work.

3.1. Surface segregation in binary alloys

Surface segregation in vacuum

For binary alloys the computational model from this work is run on a $4 \times 4 \times 100$ supercell with a configuration that is random. The temperature is ramped down from 2000 K to the final temperature over the first 5% of MC steps in order to avoid that the initial random configuration is able to end up in a local minimum energy state. The number of MC steps taken is $5 \cdot 10^5$ and the average surface fraction is taken over 20 micro states which are spaced $5 \cdot 10^3$ MC steps apart, such that they are independent of each other. This yields a standard error on the data of maximum ± 3 at.%. The energy generally converges within the first $2 \cdot 10^5$ to $3 \cdot 10^5$ MC steps.

The computational model in this thesis is based on the work by Zhao et al. [69]. Therefore, these two models are compared, as good agreement should be expected. Table 3.1 compares the models for a fixed composition against the computational developed in this thesis. The model of Zhao et al. and that of this work agree for Pd-Ag and Pd-Pt, the model deviates 4 at.% for the Pd-Cu alloy, which could be attributed to the altered elastic energy term. A difference of 5 at.% is seen for the Pd-Au alloy. Finally, a deviation of 11 at.% is found for the Pd-Ni alloy. In this alloy, the elastic energy is the dominant driving force for surface segregation. In this work a weighted average, i.e. a linear approximation, is taken for the elastic energy in order to make the elastic term anti symmetric. Furthermore, the volume of the pure elements is used instead that of the alloyed volumes to be consistent with literature.

Table 3.1: Comparison of surface segregation in five alloys in vacuum for the (111) plane at 600 K from Zhao et al. and the computational model from this work [69].

Alloy	Surface composition Zhao et al.	Surface composition this work
Pd ₇₅ Ag ₂₅	Pd ₄₈ Ag ₅₂	Pd ₄₉ Ag ₅₁
Pd ₇₅ Au ₂₅	Pd ₂₉ Au ₇₁	Pd ₂₄ Au ₇₆
Pd ₇₅ Cu ₂₅	Pd ₇₄ Cu ₂₆	Pd ₆₉ Cu ₃₁
Pd ₇₅ Ni ₂₅	Pd ₉₇ Ni ₃	Pd ₈₆ Ni ₁₄
Pd ₇₅ Pt ₂₅	Pd ₉₉ Pt ₁	Pd ₁₀₀ Pt ₀

Surface segregation is plotted for the alloys Pd-Ag, Pd-Au, Pd-Cu, Pd-Ni and Pd-Pt at 600K, shown in figure 3.1. The x-axis shows the bulk atomic fraction and the y-axis depicts the surface fraction. Strong

segregation of Au and Ag is predicted and a small segregation of Cu is predicted. A bcc region exists for the Pd-Cu alloy at a composition of 35 at.% - 45 at.% Pd [82]. However, Zhao et al. show that the segregation is not influenced significantly in this region [69]. In Pd-Ag the largest oscillation of elements in subsurface layers is seen, which is caused by the relatively large negative alloy parameter as shown in figure 3.1a. For Pd-Cu alloy, the segregation can be either Pd or Cu, depending on the composition as shown in figure 3.1c. The same is seen in the Pd-Ni system, but the larger alloying parameter results in a lower subsurface enrichment of Pd as seen in figure 3.1d. For the Pd-Pt alloy the positive alloy parameter results in the attraction of like atoms, in this case Pd-Pd and Pt-Pt as shown in figure 3.1e. Pt segregates to the surface and the first 3 to 4 atomic layers are also enriched in Pt.

Table 3.2 compares surface segregation results of Pd alloys from literature against results obtained with the present model. These results all agree within 10 at.% with the exception of $\text{Pd}_{67}\text{Ag}_{33}$, $\text{Pd}_{70}\text{Ag}_{30}$, and the Pd-Ni alloys.

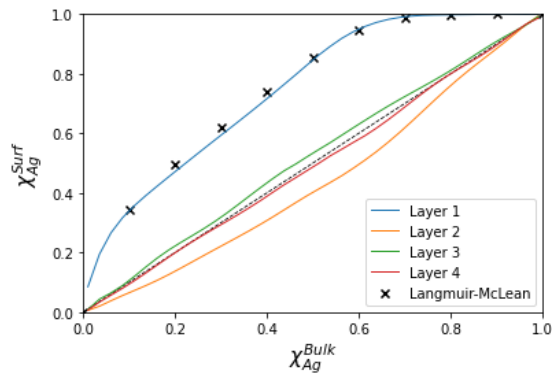
The results of Ropo et al. who studied the $\text{Pd}_{70}\text{Ag}_{30}$ alloy at 600 K and 900 K and Wouda et al. who studied $\text{Pd}_{67}\text{Ag}_{33}$ at 720 K and 920 K agree with each other [56], [68]. The results from Wouda et al. show a larger segregation at 920 K than at 720 K. This is contrary to what is expected, that is a lower segregation at a higher temperature, due to an increased entropy term. The composition of $\text{Pd}_{67}\text{Ag}_{33}$ is special as a very ordered structure occurs, as will be shown later. The results from the model from this work do not quantitatively match the results from literature at this composition, one explanation is the overprediction of the SRO. Pd and Ag have a relatively large negative mixing enthalpy of 30 meV according to Miedema's model and thus want to mix. Therefore, Pd can be pulled to the surface, thereby minimizing the mixing energy of the system. Including pairwise interactions between second nearest-neighbours could yield a more accurate result.

The elastic energy plays a dominant role in the Pd-Ni system, resulting in an underestimation of the segregation of Ni. Furthermore, Zhao et al. predict a Pd segregation at 600 K in vacuum over the entire compositional range of Pd-Ni. However, as shown in figure 3.2 the computational model developed in this thesis predicts either Pd or Ni segregation, depending on the composition. The equation for the elastic energy is described for dilute solutions by Abraham et al., which is utilized in the paper by Zhao et al. [69], [119]. Therefore, the predictions for Pd-Ni are not accurate. All binary alloys in vacuum follow the LM equation closely.

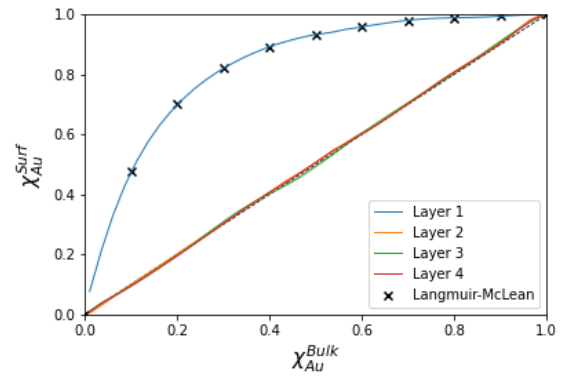
The effect of temperature on the segregation is shown in figure 3.3 for Pd-Ag and Pd-Ni. These two alloys were chosen because of their different segregation pattern. From these figures it is seen that segregation decreases with increasing temperature. The decreasing segregation can be attributed to the increasing entropy at increasing temperatures.

Short-range ordering

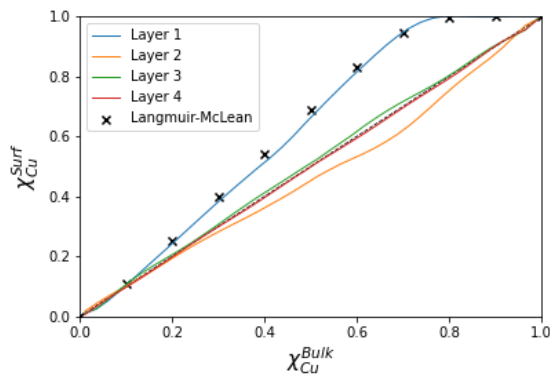
The alloy parameter ω is negative for the $\text{Pd}_{67}\text{Ag}_{33}$ alloy, therefore Pd and Ag would preferentially bind to each other. This can be observed in figure 3.4 where surface segregation was predicted for this $\text{Pd}_{67}\text{Ag}_{33}$ alloy at 0 K. In this system Ag segregation is observed, the second atomic layer is pure Pd such that the number of Pd atoms around the Ag atoms on the surface is maximized. In the third and fourth layer a slight oscillation is observed. The fifth and deeper layers are bulk like. In reality atomic movement reduces with decreasing temperatures, this results in kinetic trapping and produces thermodynamical metastable states. This not the case for the MC method applied here, thus only thermodynamical equilibrium states will be computed. This results in an overprediction of segregation or ordering at very low temperatures. At elevated temperatures SRO becomes less prominent due to the increasing entropy term. However, these ordered states also happen at a lesser degree at higher temperatures.



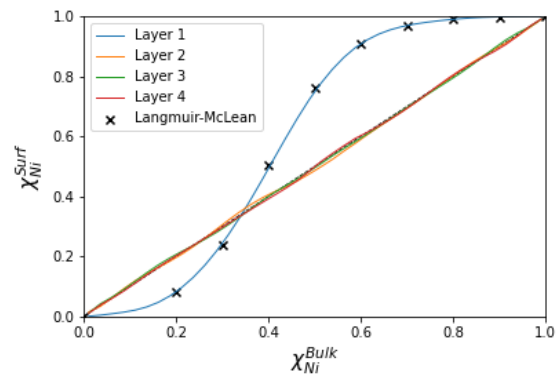
(a) Ag segregation at 600K in vacuum



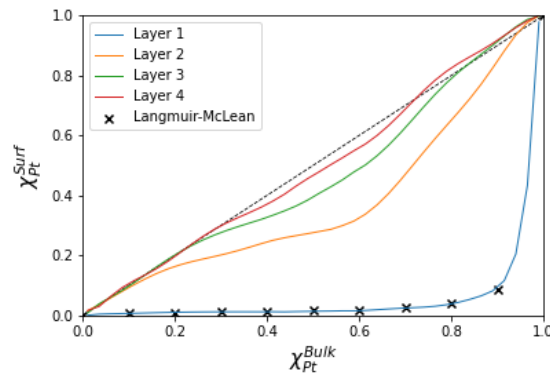
(b) Au segregation at 600K in vacuum



(c) Cu segregation at 600K in vacuum



(d) Ni segregation at 600K in vacuum



(e) Pt segregation at 600K in vacuum

Figure 3.1: Segregation of Pd-alloys in vacuum at 600K in atomic fractions of Pd-Ag, Pd-Au, Pd-Cu, Pd-Ni and Pd-Pt. The no-segregation line is indicated by the dotted line, the bulk atomic fraction of the alloying element is plotted against that of the surface. Atomic fractions above the dotted line indicate surface segregation of the alloying element. The colored lines are predicted by Miedema's model in combination with MC simulations. The crosses indicate predictions of the surface fraction by Miedema's model in combination with the LM equation.

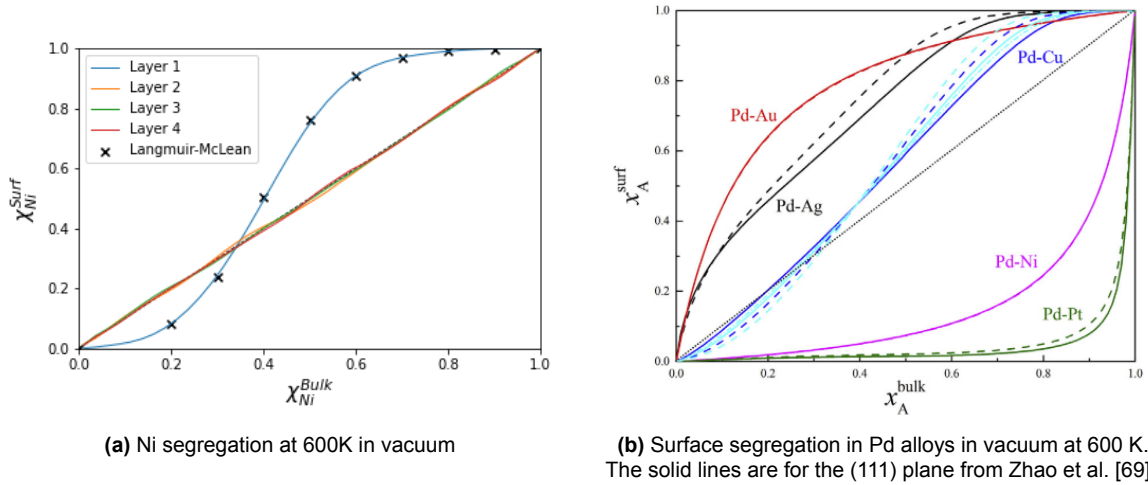


Figure 3.2: Comparison of Pd-Ni segregation at 600K. The no-segregation line is indicated by the dotted line, the bulk atomic fraction of the alloying element is plotted against that of the surface. Atomic fractions above the dotted line indicate surface segregation of the alloying element. The colored lines are predicted by Miedema's model in combination with MC simulations.

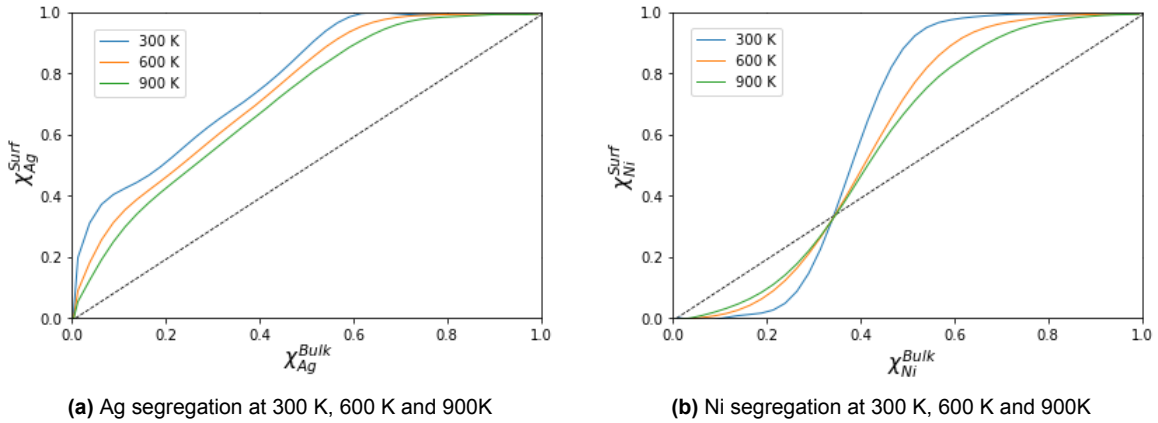


Figure 3.3: Surface segregation is compared at various temperatures for Pd-Ag and Pd-Ni, which shows that segregation increases at lower temperatures. The no-segregation line is indicated by the dotted line, the bulk atomic fraction of the alloying element is plotted against that of the surface. Atomic fractions above the dotted line indicate surface segregation of the alloying element. The colored lines are predicted by Miedema's model in combination with MC simulations.

Table 3.2: Surface segregation reported in literature compared to the predictions from this work. *Modified mean field model that includes subsurface layers.

Ref.	Method	T (K)	Composition bulk (at.%)	Surface composition literature (at.%)	Surface composition this work (at.%)
Wouda [68]	STM	720	Pd ₆₇ Ag ₃₃	Pd ₅ Ag ₉₅	Pd ₄₁ Ag ₅₉
		920	Pd ₆₇ Ag ₃₃	Pd ₁₁ Ag ₈₉	Pd ₃₈ Ag ₆₂
Ropo [56]	DFT + Mean field*	600	Pd ₇₀ Ag ₃₀	Pd ₁₂ Ag ₈₈	Pd ₄₁ Ag ₅₉
		900	Pd ₇₀ Ag ₃₀	Pd ₂₀ Ag ₈₀	Pd ₄₅ Ag ₅₅
		600	Pd ₅₀ Ag ₅₀	Pd ₁₀ Ag ₉₀	Pd ₁₈ Ag ₈₂
		900	Pd ₅₀ Ag ₅₀	Pd ₁₅ Ag ₈₅	Pd ₁₉ Ag ₈₁
		900	Pd ₃₀ Ag ₇₀	Pd ₃ Ag ₉₇	Pd ₂ Ag ₉₈
Ropo [71]	DFT + LM	0	Pd ₅₀ Ag ₅₀	Pd ₀ Ag ₁₀₀	Pd ₀ Ag ₁₀₀
		300	Pd ₅₀ Ag ₅₀	Pd ₈ Ag ₉₂	Pd ₁₀ Ag ₉₀
		600	Pd ₅₀ Ag ₅₀	Pd ₁₉ Ag ₈₁	Pd ₁₈ Ag ₈₂
		900	Pd ₅₀ Ag ₅₀	Pd ₂₅ Ag ₇₅	Pd ₁₉ Ag ₈₁
		1200	Pd ₅₀ Ag ₅₀	Pd ₂₈ Ag ₇₂	Pd ₂₇ Ag ₇₃
Yi [67]	LEIS, XPS	800	Pd ₅₀ Au ₅₀	Pd ₁₈ Au ₈₂	Pd ₁₂ Au ₈₈
			Pd ₂₅ Au ₇₅	Pd ₆ Au ₉₄	Pd ₄ Au ₉₆
			Pd ₇₅ Au ₂₅	Pd ₃₅ Au ₆₅	Pd ₃₄ Au ₆₆
Swartzfager [81]	LEIS	875	Pd ₄₀ Au ₆₀	Pd ₅ Au ₉₅	Pd ₉ Au ₉₁
			Pd ₆₀ Au ₄₀	Pd ₃₀ Au ₇₀	Pd ₂₁ Au ₇₉
Zhao [76]	Miedema + LM	800	Pd ₅₀ Au ₅₀	Pd ₂₀ Au ₈₀	Pd ₁₂ Au ₈₈
Zhao [76]	LEIS, XPS	1000	Pd ₆₀ Cu ₄₀	Pd ₅₀ Cu ₅₀	Pd ₄₉ Cu ₅₁
Priyadarshini [85]	LEIS, XPS	700	Pd ₄₈ Cu ₅₂	Pd ₂₀ Cu ₈₀	Pd ₃₂ Cu ₆₈
		900	Pd ₄₈ Cu ₅₂	Pd ₂₄ Cu ₇₆	Pd ₃₁ Cu ₆₉
		700	Pd ₄₀ Cu ₆₀	Pd ₁₇ Cu ₈₃	Pd ₂₀ Cu ₈₀
		900	Pd ₄₀ Cu ₆₀	Pd ₁₉ Cu ₈₁	Pd ₁₉ Cu ₈₁
Michel [94]	LEIS, XPS	900	Pd ₈ Ni ₉₂	Pd ₇₆ Ni ₂₄	Pd ₀ Ni ₁₀₀
Miegge [95]	LEIS, XPS	870	Pd ₁ Ni ₉₉	Pd ₂₀ Ni ₈₀	Pd ₀ Ni ₁₀₀
			Pd ₅ Ni ₉₅	Pd ₅₀ Ni ₅₀	Pd ₀ Ni ₁₀₀

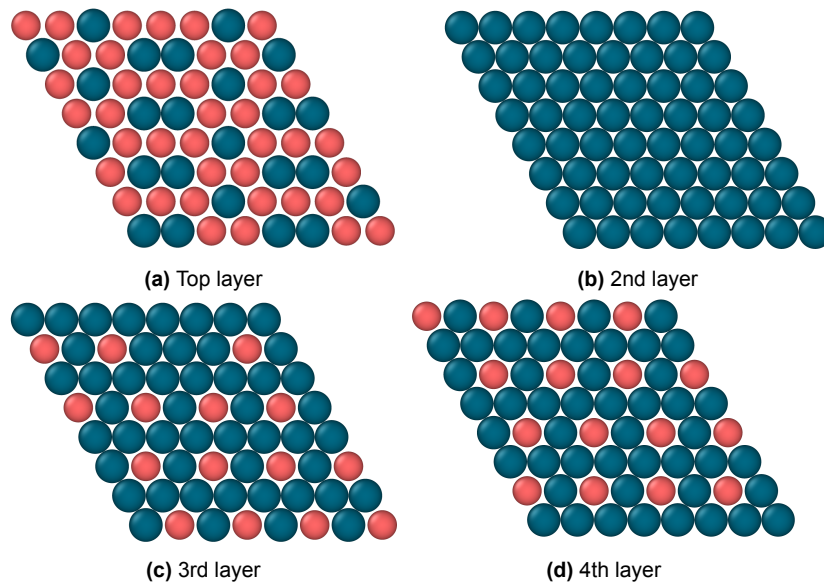
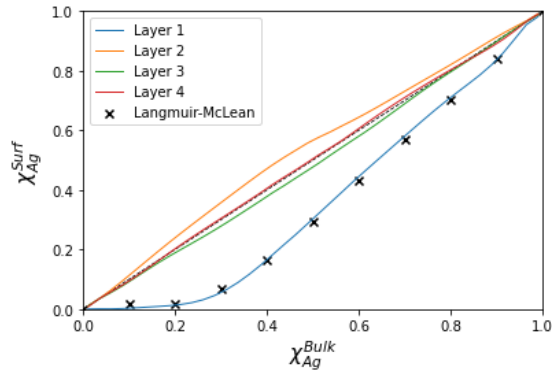


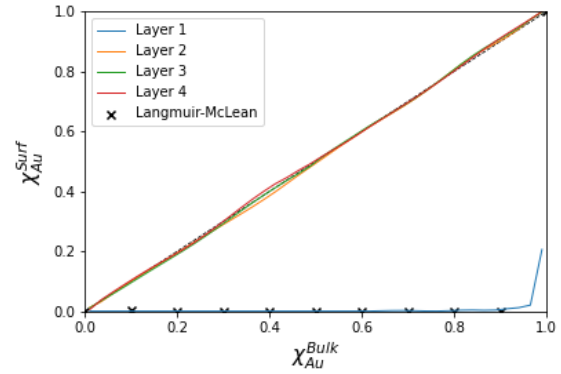
Figure 3.4: Short-range ordering in $\text{Pd}_{67}\text{Ag}_{33}$ at 0 K in vacuum for the top four atomic layers of a $8 \times 8 \times 150$ supercell.

Surface segregation with hydrogen adsorption

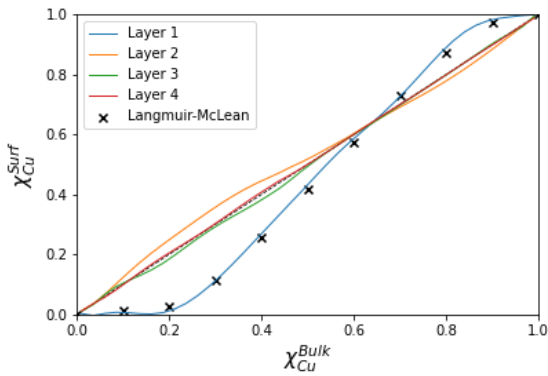
The computational model is run at 600K on a $4 \times 4 \times 100$ supercell and the (111) plane is considered. Figure 3.1 shows the segregation behavior of Pd-Ag, Pd-Au, Pd-Cu, Pd-Ni and Pd-Pt with a monolayer hydrogen by applying a pressure of $P/P_0=50$. All the other variables are kept the same as what was used for the prediction of surface segregation in vacuum. The effect of hydrogen adsorption on the surface segregation in Pd-based alloys in literature is not extensive. Zhao et al. show that Ag is depleted from the surface when hydrogen is adsorbed, similar to figure 3.5a [69]. The hydrogen coverage depends on the type of atoms that occupy the surface and vice versa. Au has an endothermic binding with hydrogen [29], therefore the Au segregation is suppressed, as can be in figure 3.5b, similar to what is presented by Zhao et al. [69]. The effect of the elastic energy in the Pd-Cu alloy is relatively large, which yields quantitative differences between the results from this work and those of Zhao et al. Zhao et al. report a lower segregation at low Cu concentrations compared to the work here, shown in figure 3.5c. Hydrogen adsorption does not have a significant effect on the segregation behaviour and this shows in the work of Zhao et al. and this work, shown in figure 3.5d. Lastly in the Pd-Pt alloy, a stronger segregation of Pt is observed when hydrogen adsorption is considered, shown in figure 3.5e, similar to the results of Zhao et al.



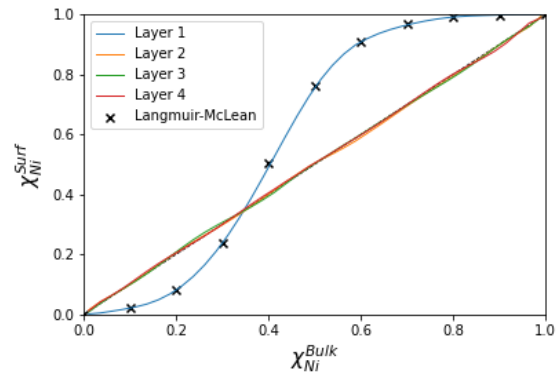
(a) Ag segregation at 600K in a hydrogen atmosphere



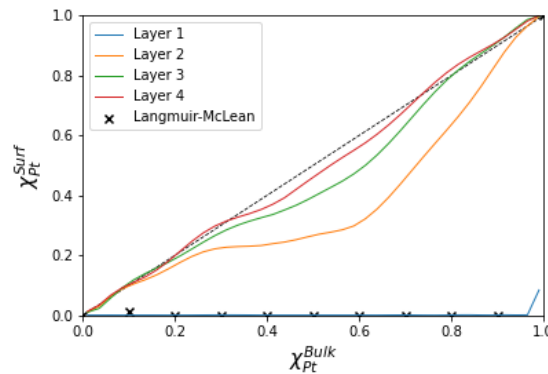
(b) Au segregation at 600K in a hydrogen atmosphere



(c) Cu segregation at 600K in a hydrogen atmosphere



(d) Ni segregation at 600K in a hydrogen atmosphere



(e) Pt segregation at 600K in a hydrogen atmosphere

Figure 3.5: Surface segregation in Pd-alloys with a monolayer hydrogen adsorbed at 600K in atomic fractions of Pd-Ag, Pd-Au, Pd-Cu, Pd-Ni and Pd-Pt. The no-segregation line is indicated by the dotted line, the bulk atomic fraction of the alloying element is plotted against that of the surface. Atomic fractions above the dotted line indicate surface segregation of the alloying element. The colored lines are predicted by Miedema's model in combination with MC simulations. The crosses indicate predictions of the surface fraction by Miedema's model in combination with the LM equation.

Conclusion on verification of binary computational model

Combining DFT with MC simulations has been employed by Ruban et al. [57] and Boes et al. [48] and have yielded accurate results for predicting the surface segregation. Unfortunately, these type of calculations are computationally intensive, which makes this approach unsuitable for fast screening of novel alloys. Literature on the TB-model is not extensive, which makes verifying its accuracy difficult. The TB-model is however also relatively computationally intensive. EAM, MEAM and Miedema's model can

be used with sufficient accuracy, but Miedema's model does not require fitting of interatomic potentials for computing the segregation enthalpy at the cost of some accuracy. MC simulations could yield more accurate results than the LM equation when SRO has an effect. However, as was shown, in binary alloys the difference between MC simulations and the LM equation are negligible.

3.2. Surface segregation in ternary alloys

The results from literature are compared against the computational model from this work. The model from this work is run with $2 \cdot 10^6$ MC steps on a $4 \times 4 \times 100$ supercell for ternary alloys and the average surface fraction is taken over 100 micro states which are spaced $5 \cdot 10^4$ MC steps apart, such that they are independent of each other. The first two sections focus on Pd-Cu-Au and Pd-Cu-Ag ternary alloys, which have seen considerable attention due to their resistance against H_2S poisoning as a result of the alloying elements Au and Cu. Furthermore, the addition of Ag leads to an improved permeability.

Effect of co-segregation, site-competition and blocking

The solute elements in a ternary alloy can interact by either attracting or repelling each other by different processes, such as co-segregation, site-competition and blocking [106]. Co-segregation describes the effect of two elements segregating to the surface as a result of a low surface energy compared to the third element, which remains in the bulk. Co-segregation increases when the bonding between the two surface elements increases or when the repulsive interaction between the third element increases. Site-competition occurs when two elements want to segregate and one of the two elements has a strong bonding with the third element, leading to a segregation of the other element. Lastly, blocking takes place when one element has a low surface energy but also binds strongly with an element that has a high surface energy. The element with the intermediate surface energy will then segregate.

The mean field assumptions of the LM equation do not consider these types of interactions and thus do not always yield accurate results. An example of this is shown in figure 3.6. The predicted surface composition by the LM equation (crosses), of La differs by 41 at.% when compared against the MC simulations (filled circles). The alloy parameter of Cu-Pd and Cu-La is large and negative (thus want to mix) and about 5 times more negative than Pd-La. Cu therefore stays in the bulk, in order to maximize the amount of La and Pd neighbors. Furthermore, La has a larger volume than both Cu and Pd, resulting in an elastic energy that pushes La to the surface. However, the alloy parameter between Pd-La is large in comparison to the elastic energy and the surface energy. Therefore blocking occurs and the segregation of La is lower than predicted by the LM equation. The surface energy in this alloy is small enough in comparison to the alloy parameter and the elastic energy that it has a negligible effect. In conclusion, predicting the surface segregation is more difficult in ternary alloys. Contrary to binary alloys, differences arise between the LM equation and MC simulations when predicting surface segregation. MC simulations will yield more accurate results as they can account for co-segregation, blocking and site-competition.

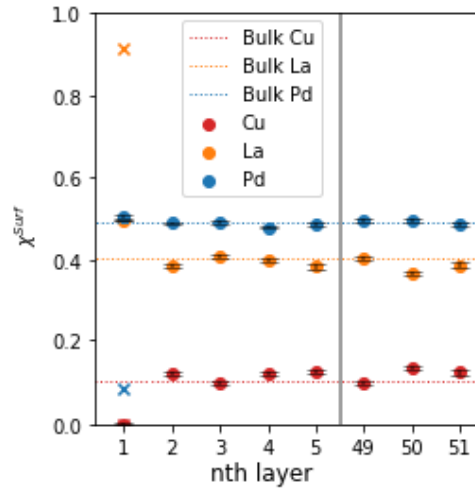


Figure 3.6: Predicted atomic fraction at the surface in $\text{Pd}_{50}\text{Cu}_{10}\text{La}_{40}$ at 600 K in vacuum by the LM equation (crosses) and by MC simulations (filled circles). Layer 49 to 51 shows the bulk composition.

Surface segregation in Pd-Cu-Au

Yin et al. [99] studied surface segregation in Pd-Cu-Au and report consistent Au segregation at a temperature of 500 K and 600 K. Furthermore, at low Au concentrations, a segregation of Cu is also observed as shown in figure 3.7. Figure 3.8 shows the predicted excess surface segregation by the computational model from this work. Please note that the maxima and minima of the colour scales are different. It must be pointed out that a wide bcc region exists in the region shown in the figures, this is outlined in red [28]. However, as shown by Zhao et al. the effect on the predicted surface segregation between fcc and bcc in the Pd-Cu alloy is approximately 5 at.% maximum and the figure can therefore still be used to qualitatively predict surface segregation [69]. Furthermore, the computational model from this work predicts phase separation in the regions that are white. It is observed that at 500 K the phase separation region for high Cu concentrations is larger. The results from Yin et al. qualitatively match the results obtained from the computational model. Pd depletion from the surface is seen throughout the entire compositional range of the Pd-Cu-Au alloy. At a composition near $\text{Pd}_{80}\text{Cu}_0\text{Au}_{20}$ a peak is seen in the depletion of Pd from the surface by both Yin et al. and by the model from this work at 500 K. Yin et al. report surface segregation of Cu at lower Au concentrations, which qualitatively match the results from this work. However, the Cu depletion from the surface at lower Cu concentrations, observed by Yin et al., is not seen. Furthermore, segregation is always observed by Yin et al., while the computational model from this work predicts a depletion of Au of up to 20 at.%. Yin et al. predict an increased segregation at higher temperatures, it is expected that this is the result of performing measurements while the alloy is in a metastable state and could explain the quantitative differences in the predicted surface segregation. In contrast, the model from this work predicts increased surface segregation at lower temperatures as a result of the lower entropy term.

Figure 3.8 outlines a region in green at a composition of $\text{Pd}_{50}\text{Cu}_{40}\text{Au}_{10}$ at 500 K. This region is less depleted in Pd than the surrounding compositions and is seen in both the results from Yin et al. and the current work. Scanning over the compositional range of $\text{Pd}_{50-x}\text{Cu}_x\text{Au}_{10}$ where x is varied between 30-50at.% the alloying parameter of Cu-Au becomes less negative with increasing Cu content while the alloying parameter of Au-Pd becomes more negative. At a composition of approximately $\text{Pd}_{44}\text{Cu}_{46}\text{Au}_{10}$ the two alloying parameters are equal. Similarly, scanning over the compositional range of $\text{Pd}_{50-y}\text{Cu}_{40}\text{Au}_y$ where y is varied between 0-20 at.%, the alloying parameter of Cu-Au becomes less negative at a large rate with increasing Au content. The alloying parameter of Au-Pd also becomes less negative with increasing Au content, albeit at a lower rate and is equal to the alloying parameter of Cu-Au at a composition of $\text{Pd}_{39}\text{Cu}_{40}\text{Au}_{21}$. The bonding of Cu-Pd remains almost unchanged in these compositional ranges. Thus, adding more Cu leads to a less strong bonding energy of Cu-Au and a stronger bonding of Au-Pd. Adding more Au leads to a less strong bonding of Cu-Au and a less strong bonding of Au-Pd. A region exists where the bonding of both Au-Pd and Au-Cu is large and thus Au

wants to remain in the bulk. This allows Pd to have a small compositional region where the surface depletion is lower.

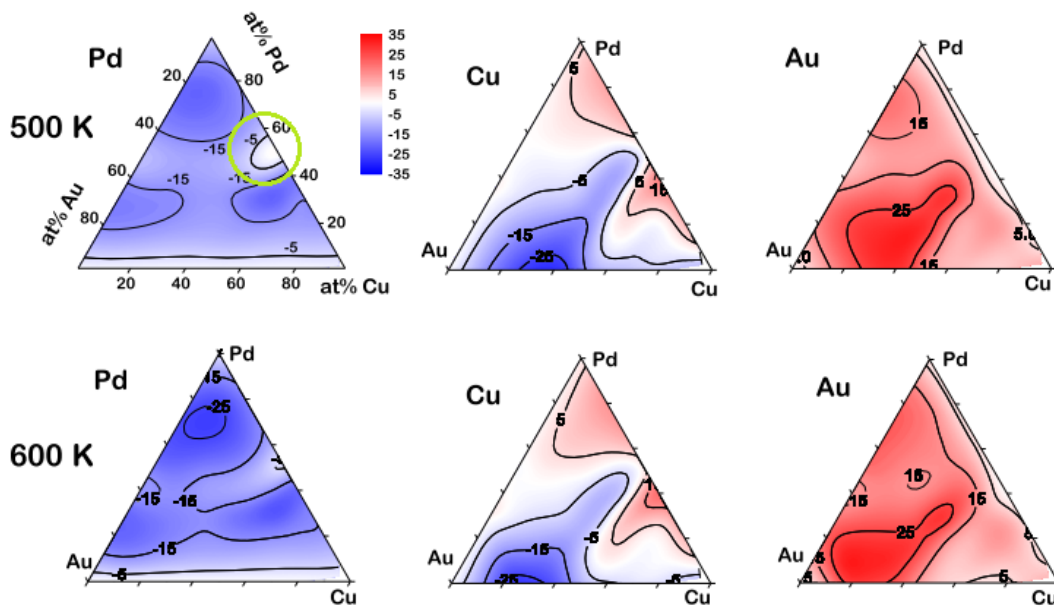


Figure 3.7: Ternary diagrams showing excess surface segregation in Pd-Cu-Au. Blue regions indicate depletion of the element from the surface while red regions show enrichment of the element on the surface. A region of lower Pd depletion than its surroundings is outlined in green from Yin et al. [99].

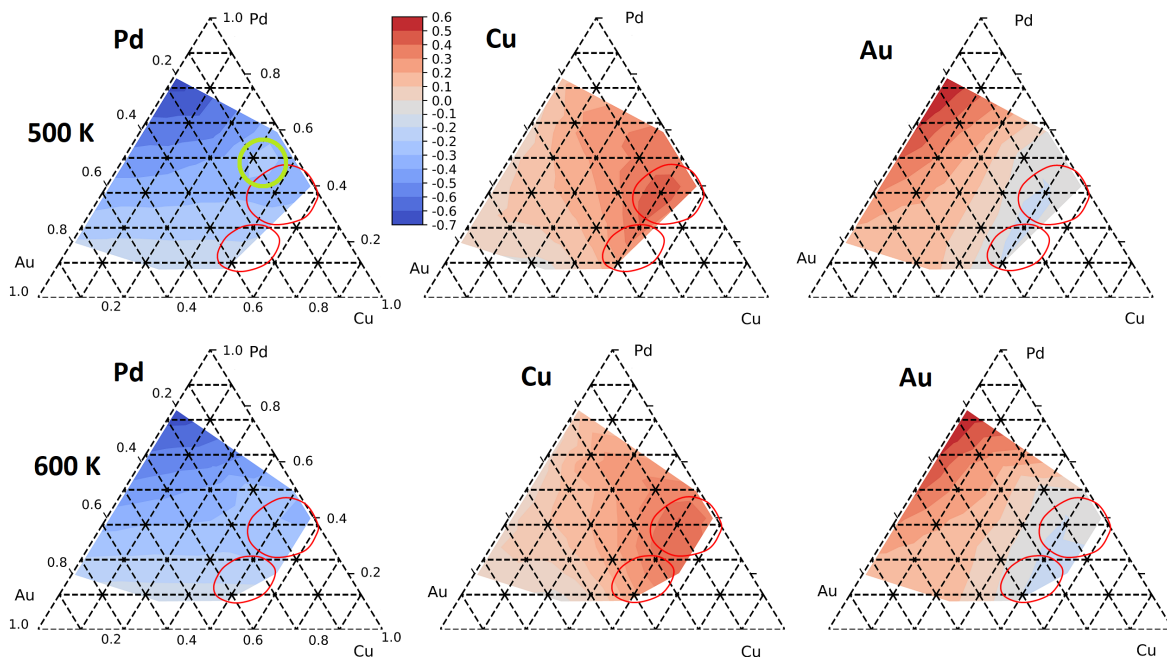


Figure 3.8: Predicted excess atomic fraction at the surface in Pd-Cu-Au at 600 K. Blue regions indicate depletion of the element from the surface while red regions show enrichment of the element on the surface. Phase separation is predicted in the regions that are left white. Bcc regions are outlined roughly in red. A region of lower Pd depletion than its surroundings is outlined in green.

Surface segregation in Pd-Cu-Ag

Zhao et al. performed experiments on the surface segregation in $\text{Pd}_{61}\text{Cu}_{29}\text{Ag}_{10}$ in vacuum at 1000 K and report a surface composition of $\text{Pd}_{39}\text{Cu}_{45}\text{Ag}_{15}$ experimentally and $\text{Pd}_{54}\text{Cu}_{54}\text{Ag}_{17}$ using a computational method which combines Miedema's model with the LM equation [103]. Thus, Cu and Ag surface segregate and Pd is depleted from the surface and the segregation is qualitatively predicted correctly. The computational method from this work predicts a surface composition of $\text{Pd}_8\text{Cu}_{67}\text{Ag}_{25}$ and thus matches the results from Zhao et al. qualitatively as shown in table 3.3. In a hydrogen atmosphere, Zhao et al. find and predict a Ag depletion and experimentally a Cu depletion, while in computations the Cu composition on the surface remains the same. The computational method from this work qualitatively agrees with the experimental results reported by Zhao et al. the model from this work has a coverage of 2/3 monolayer hydrogen compared to the monolayer coverage of Zhao et al. The diffusion kinetics might limit the surface segregation in the experimental results. Furthermore, phase separation is observed in the model from this work. Applying the SSOL2 database from Thermo-Calc a single fcc phase is however predicted [129].

Table 3.3: Reported segregation of Pd-Ag-Cu from Zhao et al. of the surface layer measured with LEIS and calculated using Miedema's model in combination with the LM equation in vacuum and with a monolayer coverage [103]. This is compared to the computational model from this work in vacuum and a 2/3 monolayer coverage of hydrogen.

Condition	Experimental Composition (at.%)		Calculated Composition Zhao et al. (at.%)		Calculated Composition This work (at.%)	
	Cu	Ag	Cu	Ag	Cu	Ag
Before segregation	29.4	10.4	30.0	10.0	29.4	10.4
1000 K in vacuum	45.1	15.3	54.4	16.5	67.3	25.0
1000 K in 1 bar H_2	23.2	7.6	29.9	3.9	9.0	0.0

Surface segregation in other ternary alloys

Zhao et al. performed experiments and developed a computational model in order to predict surface segregation in Pd-Cu-Mo. The predictions of surface segregation from Zhao et al. and those of this work are compared in table 3.4. Mo depletion is seen in both the experiments and the computational predictions in vacuum and a hydrogen atmosphere. Albeit, at a lesser degree for the experimental results as a result of diffusion kinetics. The computational model of Zhao et al. predicts a Cu depletion as well, in contrast to what the experiments show. The computational model of Zhao et al. agrees with the results from the computational model from this work. Phase separation is seen in the computational model from this work. Thermo-Calc is used in combination with the SSOL2 database, which predicts a fcc phase, together with a 2% mole fraction of bcc [129]. Therefore, the predictions by the computational model from this work could deviate from experimental results. Although Cu has a lower surface energy than Pd, the large negative alloy parameter between Cu-Mo and the relatively high surface energy of Mo would result in blocking. Thereby, still depleting Cu from the surface, resulting in surface segregation of Pd.

Table 3.4: Reported segregation of Pd-Cu-Mo from Zhao et al. of the surface layer measured with LEIS and calculated using Miedema's model in combination with the LM equation in vacuum and with a monolayer coverage [103]. This is compared to the computational model from this work in vacuum and a 2/3 monolayer coverage of hydrogen.

Condition	Experimental Composition (at.%)		Calculated Composition Zhao et al. (at.%)		Calculated Composition This work (at.%)	
	Cu	Mo	Cu	Mo	Cu	Mo
Before segregation	5.2	10.9	5	10	5.2	10.9
1000 K in vacuum	6.0	3.6	0	0	0	0
1000 K in 1 bar H ₂	5.2	4.5	0	0	0	0

Luyten et al. derive parameters for the MEAM for Pt₂₀Pd₄₀Rh₄₀ [106]. The potential is then validated on the (111) plane at various temperatures using MC simulations. At 1200 K a surface composition is predicted of Pt₁₀Pd₈₉Rh₁, the model from this work predicts a surface composition of Pt₇Pd₈₇Rh₆. These models agree quantitatively with a maximum deviation of 5 at.% Rh. At 600 K Luyten et al. report a predicted surface composition of Pt₂Pd₉₈Rh₀ and the model from this work predicts a surface composition of Pt₂Pd₉₇Rh₁, which agrees well.

Yu et al. used the modified analytical embedded atom method in combination with MC simulations to predict surface segregation in four Pd-Pt-Rh alloys at 1200 K, these are compared in table 3.5 against the results from this work [105]. Yu et al. report qualitative agreement between their model and other literature. The results from the model from this work agrees qualitatively with the results from Yu et al.

Table 3.5: Surface segregation predicted by Yu et al. in four Pd-Pt-Rh alloys at 1200 K compared to the predicted surface segregation from this work [105].

Bulk Composition (at.%)	Calculated Composition Yu et al. (at.%)		Calculated Composition This work (at.%)	
	Pd	Rh	Pd	Rh
Pt ₂₅ Pd ₅ Rh ₇₀	94	6	15	57
Pt ₁₀ Pd ₁₅ Rh ₇₅	90	10	53	40
Pt ₈₀ Pd ₁₅ Rh ₅	21	0	50	2
Pt ₇₅ Pd ₁₀ Rh ₁₅	48	0	32	10

Conclusion on verification of ternary computational model

Co-segregation, site-competition and blocking can play a dominant role in the surface segregation in ternary alloys. Therefore, MC simulations should be used instead of applying the LM equation. The literature for surface segregation in ternary alloys is not extensive. Qualitative agreement is reported between the results obtained by this work and the available literature, with the exception of the experimental results in Pd-Cu-Mo obtained by Zhao et al. [103]. Generally, the predicted surface segregation from this work is higher than that of experimental results. The computational model from this work predicts the surface segregation for an alloy that is in complete thermodynamical stability. Whereas experiments generally measure the surface segregation in an alloy that is in a metastable state, resulting in a less pronounced segregation.

4

Designing surface alloys

The model discussed in the previous chapters will now be applied to design new Pd-based hydrogen separation membranes. Pd is chosen because of its intrinsic capabilities of hydrogen dissociation from the molecular form into a monoatomic form. Furthermore, Pd is capable of adsorbing approximately 600 times its own volume in hydrogen whilst maintaining its physical properties and structural integrity [17].



Figure 4.1: Approach to tailor the surface composition of a ternary alloy.

Cu is added to the alloy in order to improve the surface poisoning resistance. The drawback of Pd-Cu membranes is their relatively low permeability whilst staying in the fcc phase. Chapter 1 showed that Ag can improve the permeability. However, Cu and Ag co-segregate in vacuum or low coverages of hydrogen in the Pd-Cu-Ag alloy as was shown by the computational method from this work in the previous chapter and by experimental in combination with a computational method by Zhao et al. [103]. As hydrogen does not preferentially adsorb on Ag sites, the number of hydrogen adsorption sites is reduced. Therefore, the model can be applied to improve the permeability of the Pd-Cu alloy by adding another element. A selection can be made of elements that not only improve the permeability but are also relatively cheap, in order to reduce material cost. Figure 4.1 shows the approach that is taken to develop a novel ternary alloy that can be applied as a hydrogen separation membrane. For these Pd-Cu-X alloys Thermo-Calc and the database "SSOL 2: SGTE alloy solutions Database v2.1" is used to determine the phase diagrams to find the compositional range in which the alloys remains in a single

fcc phase for 600 K, 800 K and 1000 K [128], [129]. The elements which have a narrow fcc region or no fcc region at all are coloured red and the elements that reduce the permeability are coloured grey. Lastly, the elements that are as expensive as Pd or radioactive are coloured orange. This leaves three elements; Zr, Hf and La. The selection process is shown in figure 4.2.

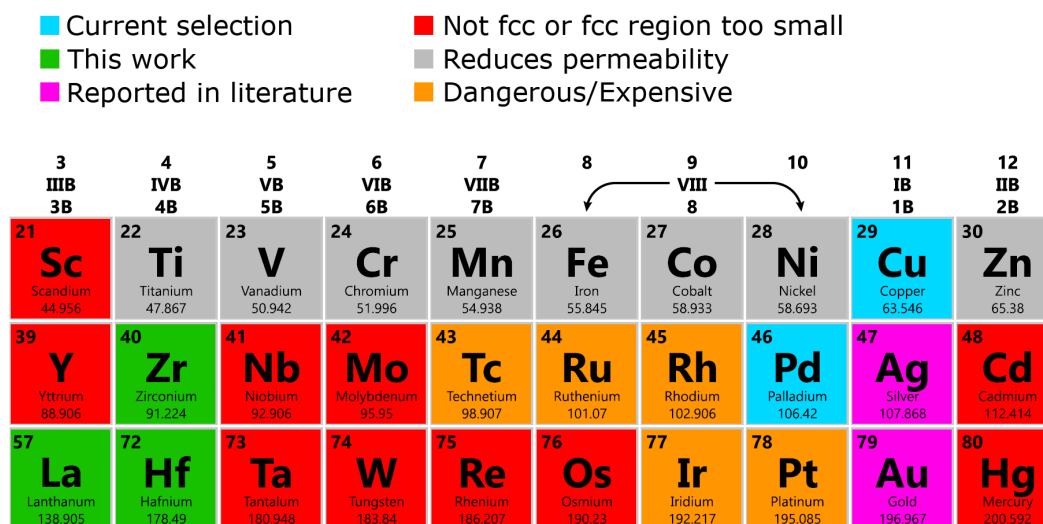


Figure 4.2: Approach to find transition metal that can improve the permeability of the Pd-Cu alloy.

Zr and Hf are chemically very similar, as Hf is more expensive it is disregarded as well [130]. ThermoCalc and the aforementioned SSOL database, predict a single fcc region at all Pd-Cu-La concentrations at every temperature. Nayebossadri et al. have shown that a bcc region exists in Pd-Cu alloys for Pd concentrations between 35 at.% to 47 at.% at temperatures below 600 K [82]. Reducing the La content to 0.1 at.% with 39.9 at.% Pd and 60 at.% at 400 K should yield a bcc structure. This is however not predicted by Thermo-Calc, the results from running the model from this work for the Pd-Cu-La alloy could therefore predict inaccurate surface segregation and is therefore not shown. Furthermore, no phase diagram is available in literature for Pd-Cu-La to the authors knowledge. For this reason, the focus of the remainder of this chapter is rather on the very promising Pd-Cu-Zr alloy.

First a 'roughing pass' of MC simulations are run for the compositional range of Pd-Cu-Zr alloy that stay in the fcc region at 600 K, 800 K and 1000 K, which are shown in figure 4.3. At increasing temperatures, the fraction of Zr can be increased while staying in the fcc region. Steps of 2 at.% were taken in Zr and 7 at.% for Cu on a 4x4x100 supercell and $2 \cdot 10^5$ MC steps. At temperatures below 600 K, the fcc region shrinks further and the effect of the Zr on the permeability is expected to be reduced significantly. At elevated temperatures entropy increases and hydrogen is less likely to adsorb on the surface, reducing the hydrogen flux through the membrane. Alternatively, the pressure is increased in order to make hydrogen adsorb to the surface.

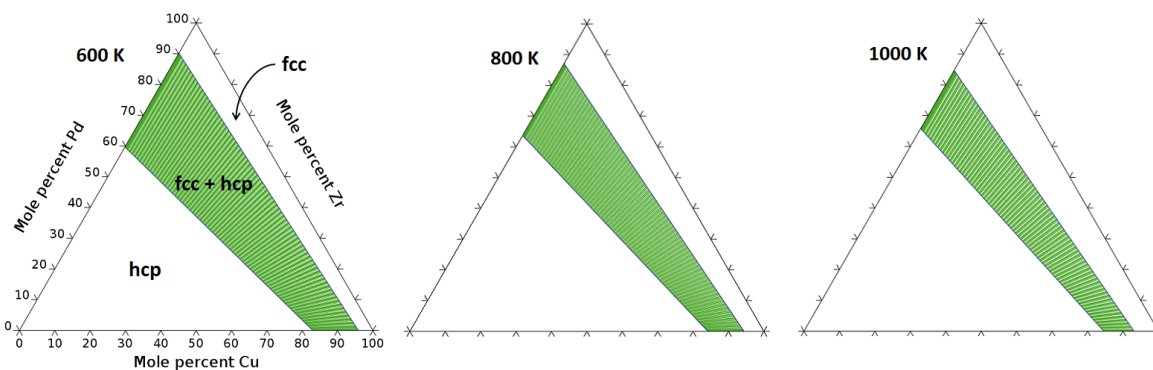


Figure 4.3: Phase diagram of Pd-Cu-Zr at 600 K, 800 K and 1000 K predicted by Thermo-Calc using the SGTE database [129].

The computational model from this work predicts that hydrogen adsorption does not occur at 800 K and 1000 K at a pressure of $P/P_0=50$ and are disregarded. The predicted segregation is shown in figure 4.4, Pd surface segregation is seen at Pd fractions of >0.5 and is increased in a hydrogen atmosphere. Cu segregation is seen for Pd fractions <0.5 and is decreased in a hydrogen atmosphere at 600 K. For the white regions no predictions of the excess atomic fraction are made. There are two reasons for this; 1. Thermo-Calc predicts the alloy to be in the fcc+hcp phase or hcp phase, as was shown in figure 4.3. 2. The computational model from this work suggests that phase separation occurs at Pd concentrations of >0.6 and <0.1 .

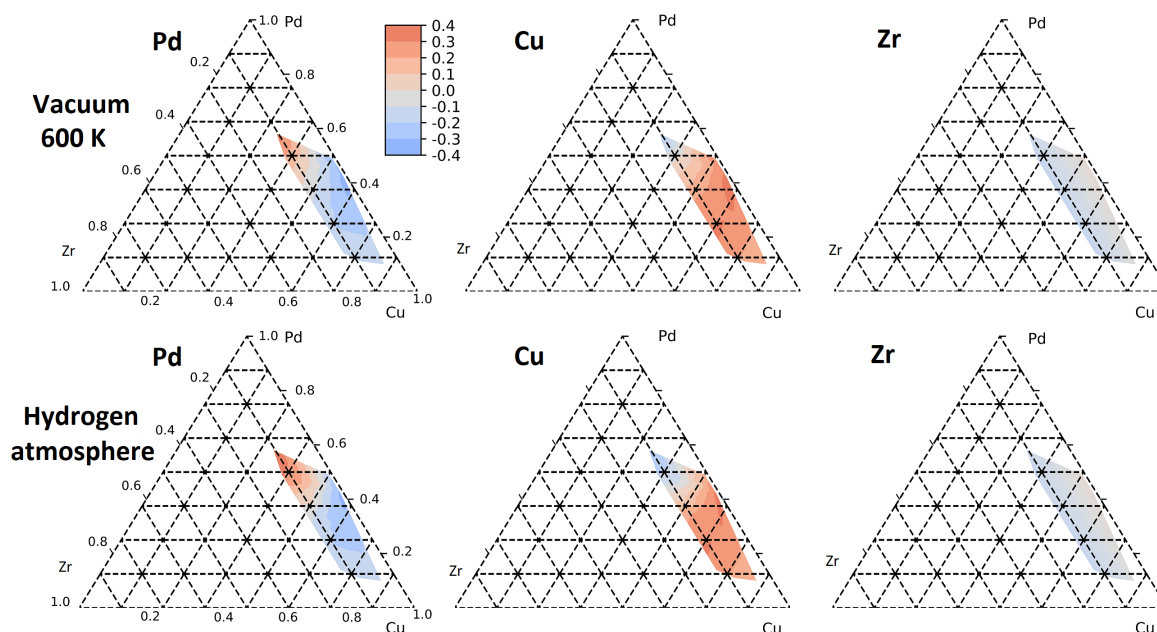


Figure 4.4: Predicted excess atomic fraction at the surface of Pd-Cu-Zr at 600 K in vacuum and a hydrogen atmosphere. Blue regions indicate depletion of the element from the surface while red regions show enrichment of the element on the surface.

The goal of this alloy is to have Zr in the bulk, to increase the permeability in combination with Pd and Cu on the surface. An additional advantage is that an addition of Zr to the Pd-H system leads to a convergence of the lattice parameters of the α and β phase, resulting in lower induced stresses, thereby reducing hydrogen embrittlement [45]. Pd on the surface is needed for the hydrogen dissociation, while Cu is needed to improve the poisoning resistance. Peters et al. report that a $\text{Pd}_{70}\text{Cu}_{30}$ membrane in a 100 ppm H_2S environment at 670 K and 770 k is able to recover completely, while a pure Pd membrane fails immediately [131]. No report is made of the surface composition, however at these temperatures and at this composition literature consistently report little to no segregation of Cu. Therefore, the surface

composition is assumed to be the same as the bulk composition, $\text{Pd}_{70}\text{Cu}_{30}$. Using the results from the 'roughing' pass, final simulations are run at 600 K for a $4 \times 4 \times 100$ supercell and $2 \cdot 10^6$ MC steps for the ternary bulk compositions that have a surface composition of around $\text{Pd}_{70}\text{Cu}_{30}$. From these simulations, the proposed bulk composition for a novel hydrogen separation membrane is $\text{Pd}_{48}\text{Cu}_{42}\text{Zr}_{10}$. This alloy has a surface composition of $\text{Pd}_{71}\text{Cu}_{29}$ in a hydrogen atmosphere, the surface composition is shown in figure 4.5. The composition on the vacuum side is $\text{Pd}_{54}\text{Cu}_{46}$, in experiments the Pd content on this surface would be higher, due to the permeated hydrogen. Note that the LM equation would have predicted a different surface composition, so it is not appropriate for ternary alloy design.

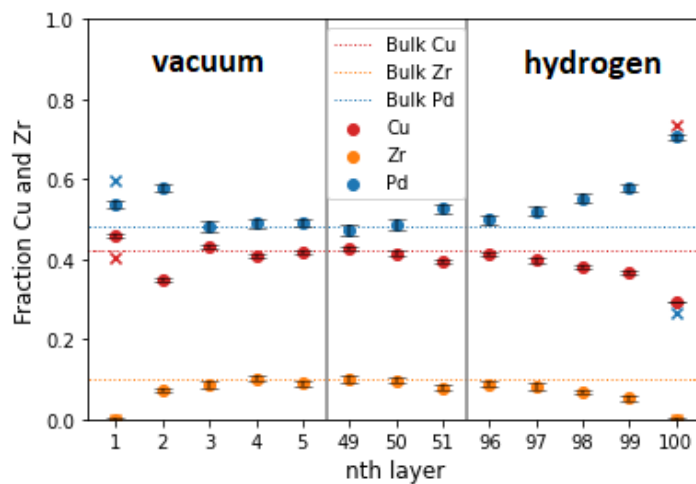


Figure 4.5: Segregation of $\text{Pd}_{48}\text{Cu}_{42}\text{Zr}_{10}$. The first layer is exposed to vacuum, the 100th layer is exposed to hydrogen. Crosses indicate the predicted segregation by the LM equation in vacuum and when exposed to a monolayer hydrogen.

5

Conclusion

Surface segregation is of great importance as the catalytic activity is mostly determined by the surface layer. For binary alloys the LM equation is a good indicator for the final surface composition. Screening a vast array of alloys using the LM equation for binary alloys is thus a more effective way to find novel binary alloys than using MC simulations. This is not the case for ternary alloys as an interplay of driving forces can affect the surface composition. Blocking, co-segregation and site-competition play an important role in determining the surface composition of ternary alloys. The computational model presented in this work is to the authors knowledge the first time that a framework has been constructed to systematically design SA's and NSA's for ternary alloys. The computational model is based on a parameterization of Miedema's model to construct pairwise interactions between nearest-neighbors which are used in MC simulations. This is a large improvement over the trial and error procedures that are currently employed which take up more time and are costlier.

The main research question is repeated below:

Are calculations using Miedema's model in combination with MC sufficiently fast and reliable to predict and screen surface segregation in ternary alloys?

In order to answer this question, two sub-questions have to be answered.

1. *How reliably can Miedema's model predict the segregation enthalpy of ternary alloys when only pairwise interactions from nearest-neighbors are considered?*

The computational model from this work finds quantitative agreement for binary alloys when the elastic energy is not dominant and qualitative agreement for ternary alloys. The computational model proposed in this work can aid in speeding up the designing process of ternary surface alloys. The model is written in order to speed up the design process of ternary alloys, as current computational methods are computationally intensive and the trial-and-error method is slow and expensive. Because literature is not available, verification of the computational model from this work is difficult.

2. *How large is the effect of deviating from a perfectly random solid solution by using Monte Carlo simulations instead of the LM equation on the predicted surface segregation?*

The LM equation is able to predict the surface segregation accurately in a binary alloy and matches the results of MC simulations generally. In ternary alloys, the LM equation can yield qualitative wrong results. Furthermore, large deviations of up to 41 at.% are seen between the LM equation and MC simulations in some alloys as a result of co-segregation, blocking or site-competition. Therefore, MC simulations should be used in ternary alloys.

By combining the answers to these questions, the main research question is answered as follows:

Surface segregation is qualitatively predicted correctly in ternary alloys by the model presented in this thesis. Quantitative conclusions cannot be drawn due to the lack of available literature. The computational model from this work allows for fast screening through the vast range of alloys to predict the surface composition qualitatively which can be used for novel catalytic surfaces. This model can be used to suggest regions of interest of an alloy at a certain temperature and pressure that should be further investigated by more computational intensive methods or experiments to obtain quantitative results. Moreover, subsurface compositions and ordering effects on the surface and subsurfaces are predicted, which is of great importance for catalytic applications.

5.1. Limitations of the computational model

It is important to realize that the model developed in this work carries various limitations.

- The accuracy of Miedema's model limits the use in predicting quantitative segregation as the average relative error is 0.37 and a correlation factor of only 0.87 is found when the correction factor of Wang is applied [114].
- The interaction energies are simplified to pairwise interactions and consider only nearest-neighbour interactions. This is the simplest approximation and the least computational intensive. Longer interactions are disregarded but can have a significant effect on the surface segregation.
- The absorption of hydrogen (and other gases) affects the surface segregation and has not been considered in the current work.
- The effect of converging to a thermodynamical equilibrium generally results in a larger surface segregation than what is seen in experiments.
- The slabs are exposed to a vacuum or to a pure hydrogen environment in the model from this work. In a real world application, the gas environment will consist of various gases which affect the surface segregation and should be added to the model.

6

Recommendations

Based on the conclusions from the previous chapter, several recommendations are made.

- Verifying the predicted surface segregation in $\text{Pd}_{48}\text{Cu}_{42}\text{Zr}_{10}$ with DFT + MC simulations and experiments. This composition is predicted to be an interesting novel hydrogen separation membrane alloy. DFT uses a different basis for the computation of the segregation enthalpy, if DFT+MC simulations predict similar segregation to the results from this work, a similar segregation would be expected in experiments.
- A single practical application of the model is shown in this thesis. However, many applications require a control over the surface composition and can thus benefit from the computational method from this work. Furthermore, the MC simulations applied in the computational method from this work predict SRO, SA's and NSA's which can be used to explore different types of promising catalytic surfaces and subsurfaces.
- Hydrogen absorption affects surface segregation. Implementing hydrogen absorption in the computational model should yield results that agree better with experiments.
- Surface segregation in vacuum and a hydrogen environment is considered in the presented model, extending this to a mixture of gases will simulate a more practical application.
- The scope of this thesis was on the fcc phase and on the (111) plane, this model can be readily modified to screen other crystal structures and crystallographic planes.
- Only pairwise interactions between nearest-neighbours are considered. The significance of second nearest-neighbours can be investigated.
- Extending the model to quaternary or quinary alloys can aid in the design of future catalytic applications.

References

- [1] H. Hoster, "Properties of Surface Alloys," in *Surface and Interface Science*, Wiley, Nov. 2013, pp. 61–100.
- [2] A. Seo, J. Lee, K. Han, and H. Kim, "Performance and stability of Pt-based ternary alloy catalysts for PEMFC," *Electrochimica Acta*, vol. 52, no. 4, pp. 1603–1611, 2006.
- [3] A. V. Ruban, H. L. Skriver, and J. K. Nørskov, "Surface segregation energies in transition-metal alloys," *Physical Review B*, vol. 59, no. 24, pp. 15 990–16 000, 1999.
- [4] J. Greeley and M. Mavrikakis, "Near-surface alloys for hydrogen fuel cell applications," *Catalysis Today*, vol. 111, no. 1-2, pp. 52–58, 2006.
- [5] J. A. Rodriguez and D. W. Goodman, "The nature of the metal-metal bond in bimetallic surfaces," *Science*, vol. 257, no. 5072, pp. 897–903, 1992.
- [6] J. C. Vickerman, K. Christmann, and G. Ertl, "Model Studies on Bimetallic Cu / Ru," *J. Catal.*, vol. 191, pp. 175–191, 1981.
- [7] J. Zhang, M. B. Vukmirovic, Y. Xu, M. Mavrikakis, and R. R. Adzic, "Controlling the catalytic activity of platinum-monolayer electrocatalysts for oxygen reduction with different substrates," *Angewandte Chemie - International Edition*, vol. 44, no. 14, pp. 2132–2135, 2005.
- [8] J. B. Henry, A. Maljusch, M. Huang, W. Schuhmann, and A. S. Bondarenko, "Thin-film Cu-Pt(111) near-surface alloys: Active electrocatalysts for the oxygen reduction reaction," *ACS Catalysis*, vol. 2, no. 7, pp. 1457–1460, 2012.
- [9] Y. Ma and P. B. Balbuena, "Pt surface segregation in bimetallic Pt₃M alloys: A density functional theory study," *Surface Science*, vol. 602, no. 1, pp. 107–113, 2008.
- [10] K. J. J. Mayrhofer, V. Juhart, K. Hartl, M. Hanzlik, and M. Arenz, "K. J. J. Mayrhofer Core–Shell Catalyst Communication 2009.pdf," *Angewandte Chemie - International Edition*, p. 3529, 2009.
- [11] Z.-J. Wang, J. Chen, Y. Huang, and Z.-X. Chen, "Surface segregation of PdM (M=Cu, Ag, Au) alloys and its implication to acetylene hydrogenation, DFT-based Monte Carlo simulations," *Materials Today Communications*, vol. 28, p. 102 475, 2021.
- [12] Q. Sun, X. Liu, Q. Han, J. Li, R. Xu, and K. Zhao, "A comparison of AA2024 and AA7150 subjected to ultrasonic shot peening: Microstructure, surface segregation and corrosion," *Surface and Coatings Technology*, vol. 337, pp. 552–560, 2018.
- [13] W. J. Wang, S. Hwang, T. Kim, S. Ha, and L. Scudiero, "Study of carbon supported CuPd alloy nanoparticles with Pd-rich surface for the electrochemical formate oxidation and CO₂ reduction," *Electrochimica Acta*, vol. 387, p. 138 531, 2021.
- [14] L. Xu, F. Xian, Y. Zhang, and L. Zhang, "Surface segregation of Ag and its effect on the microstructure, optical properties and conduction type of ZnO thin films," *Physica B: Condensed Matter*, vol. 566, pp. 103–115, 2019.
- [15] D. Fraile, J.-C. Lanoix, P. Maio, A. Rangele, and A. Torres, "Overview of the market segmentation for hydrogen across potential customer groups, based on key application areas," Tech. Rep., 2015.
- [16] ISO, "INTERNATIONAL STANDARD Hydrogen fuel — Product fuel cell applications for road vehicles," Tech. Rep., 2012.
- [17] N. A. Al-Mufachi, N. V. Rees, and R. Steinberger-Wilkens, "Hydrogen selective membranes: A review of palladium-based dense metal membranes," *Renewable and Sustainable Energy Reviews*, vol. 47, pp. 540–551, 2015.
- [18] A. M. Tarditi and L. M. Cornaglia, "Novel PdAgCu ternary alloy as promising materials for hydrogen separation membranes: Synthesis and characterization," *Surface Science*, vol. 605, no. 1-2, pp. 62–71, 2011.

- [19] B. D. Adams and A. Chen, "The role of palladium in a hydrogen economy," *Materials Today*, vol. 14, no. 6, pp. 282–289, 2011.
- [20] N. W. Ockwig and T. M. Nenoff, "Membranes for hydrogen separation," *Chemical Reviews*, vol. 107, no. 10, pp. 4078–4110, 2007.
- [21] A. Helmi, F. Gallucci, and M. Van Sint Annaland, "Resource scarcity in palladium membrane applications for carbon capture in integrated gasification combined cycle units," *International Journal of Hydrogen Energy*, vol. 39, no. 20, pp. 10 498–10 506, 2014.
- [22] F. A. Lewis, "Hydrogen in palladium and palladium alloys," *International Journal of Hydrogen Energy*, vol. 21, no. 6, pp. 461–464, 1996.
- [23] J. K. Ali, E. J. Newson, and D. W. Rippin, "Deactivation and regeneration of PdAg membranes for dehydrogenation reactions," *Journal of Membrane Science*, vol. 89, no. 1-2, pp. 171–184, 1994.
- [24] Ø. Hatlevik, S. K. Gade, M. K. Keeling, P. M. Thoen, A. P. Davidson, and J. D. Way, "Palladium and palladium alloy membranes for hydrogen separation and production: History, fabrication strategies, and current performance," *Separation and Purification Technology*, vol. 73, no. 1, pp. 59–64, 2010.
- [25] N. Pomerantz and Y. H. Ma, "The effect of H₂S on the Performance and Long-Term Stability of Pd/Cu Membranes," *Understanding Biocorrosion: Fundamentals and Applications*, vol. 1, no. 5, pp. 385–407, 2014.
- [26] C. H. Chen and Y. H. Ma, "The effect of H₂S on the performance of Pd and Pd/Au composite membrane," *Journal of Membrane Science*, vol. 362, no. 1-2, pp. 535–544, 2010.
- [27] M. V. Mundschau, X. Xie, C. R. Evenson IV, and A. F. Sammells, "Dense inorganic membranes for production of hydrogen from methane and coal with carbon dioxide sequestration," *Catalysis Today*, vol. 118, no. 1-2, pp. 12–23, 2006.
- [28] H. Jia, P. Wu, G. Zeng, E. Salas-Colera, A. Serrano, G. R. Castro, H. Xu, C. Sun, and A. Goldbach, "High-temperature stability of Pd alloy membranes containing Cu and Au," *Journal of Membrane Science*, vol. 544, pp. 151–160, 2017.
- [29] D. Tománek, S. Mukherjee, V. Kumar, and K. H. Bennemann, "Calculation of chemisorption and absorption induced surface segregation," *Surface Science*, vol. 114, no. 1, pp. 11–22, 1982.
- [30] W. Koros and G. Fleming, "Membrane-based gas separation W.J.," *Journal of Membrane Science*, vol. 83, pp. 1–80, 1993.
- [31] P. Nordlander, J. K. Norskov, and F. Besenbacher, "Trends in hydrogen heats of solution and vacancy trapping energies in transition metals," *Journal of Physics F: Metal Physics*, vol. 16, no. 9, pp. 1161–1171, 1986.
- [32] R. E. Buxbaum and T. L. Marker, "Hydrogen transport through non-porous membranes of palladium-coated niobium, tantalum and vanadium," *Journal of Membrane Science*, vol. 85, no. 1, pp. 29–38, 1993.
- [33] Stephen N. Paglieri, J. R. Wermer, R. E. Buxbaum, M. V. Ciocco, B. H. Howard, and B. D. Morreale, "Development of Membranes for Hydrogen Separation: Pd-coated V-10Pd," *Energy Materials*, vol. 3, no. 3, 2008.
- [34] B. D. Morreale, M. V. Ciocco, B. H. Howard, R. P. Killmeyer, A. V. Cugini, and R. M. Enick, "Effect of hydrogen-sulfide on the hydrogen permeance of palladium-copper alloys at elevated temperatures," *Journal of Membrane Science*, vol. 241, no. 2, pp. 219–224, 2004.
- [35] J. Okazaki, D. A. Tanaka, M. A. Tanco, Y. Wakui, F. Mizukami, and T. M. Suzuki, "Hydrogen permeability study of the thin Pd-Ag alloy membranes in the temperature range across the α - β phase transition," *Journal of Membrane Science*, vol. 282, no. 1-2, pp. 370–374, 2006.
- [36] Y. Sakamoto, F. L. Chen, M. Furukawa, and M. Noguchi, "Permeability and diffusivity of hydrogen in palladium-rich Pd-Y(Gd)-Ag ternary alloys," *Journal of Alloys and Compounds*, vol. 185, no. 2, pp. 191–205, 1992.
- [37] D. Fort, J. P. Farr, and I. R. Harris, "A comparison of palladium-silver and palladium-yttrium alloys as hydrogen separation membranes," *Journal of The Less-Common Metals*, vol. 39, no. 2, pp. 293–308, 1975.

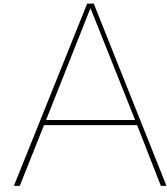
- [38] I. R. Harris and M. Norman, "The electronic state of cerium in some palladium alloys," *Journal of The Less-Common Metals*, 1968.
- [39] X. Ke, G. J. Kramer, and O. M. Løvvik, "The influence of electronic structure on hydrogen absorption in palladium alloys," *Journal of Physics Condensed Matter*, vol. 16, no. 34, pp. 6267–6277, 2004.
- [40] P. Li, Z. Wang, Z. Qiao, Y. Liu, X. Cao, W. Li, J. Wang, and S. Wang, "Recent developments in membranes for efficient hydrogen purification," *Journal of Membrane Science*, vol. 495, pp. 130–168, 2015.
- [41] G. Bernardo, T. Araújo, T. da Silva Lopes, J. Sousa, and A. Mendes, "Recent advances in membrane technologies for hydrogen purification," *International Journal of Hydrogen Energy*, vol. 45, no. 12, pp. 7313–7338, 2020.
- [42] M. D. Dolan, "Non-Pd BCC alloy membranes for industrial hydrogen separation," *Journal of Membrane Science*, vol. 362, no. 1-2, pp. 12–28, 2010.
- [43] S. K. Gade, E. A. Payzant, H. J. Park, P. M. Thoen, and J. D. Way, "The effects of fabrication and annealing on the structure and hydrogen permeation of Pd-Au binary alloy membranes," *Journal of Membrane Science*, vol. 340, no. 1-2, pp. 227–233, 2009.
- [44] J. Okazaki, T. Ikeda, D. A. Tanaka, K. Sato, T. M. Suzuki, and F. Mizukami, "An investigation of thermal stability of thin palladium-silver alloy membranes for high temperature hydrogen separation," *Journal of Membrane Science*, vol. 366, no. 1-2, pp. 212–219, 2011.
- [45] Y. Sakamoto and K. Baba, "The Effect of Alloying of Palladium on the Hydrogen-Palladium Miscibility Gap," *Zeitschrift für Physikalische Chemie*, vol. 158, no. 2, pp. 223–235, 1988.
- [46] O. Iyoha, R. Enick, R. Killmeyer, and B. Morreale, "The influence of hydrogen sulfide-to-hydrogen partial pressure ratio on the sulfidization of Pd and 70 mol% Pd-Cu membranes," *Journal of Membrane Science*, vol. 305, no. 1-2, pp. 77–92, 2007.
- [47] M. L. Bosko, A. Dalla Fontana, A. M. Tarditi, and L. Cornaglia, "Advances in hydrogen selective membranes based on palladium ternary alloys," *International Journal of Hydrogen Energy*, vol. 46, no. 29, pp. 15 572–15 594, 2021.
- [48] J. R. Boes and J. R. Kitchin, "Modeling Segregation on AuPd(111) Surfaces with Density Functional Theory and Monte Carlo Simulations," *Journal of Physical Chemistry C*, vol. 121, no. 6, pp. 3479–3487, 2017.
- [49] S. Daw, Murray, M. Foiles, Stephen, and I. Baskes, Michael, "The embedded-atom method : a review of theory and applications," *Materials Science Reports*, vol. 9, pp. 251–310, 1993.
- [50] P. Ray and M. Akinc, "Estimation of Formation Enthalpies Using An Extended Miedema Approach," in *22nd Annual Conference on Fossil Energy Materials*, 2008.
- [51] J. F. Herbst, "On extending Miedema's model to predict hydrogen content in binary and ternary hydrides," *Journal of Alloys and Compounds*, vol. 337, no. 1-2, pp. 99–107, 2002.
- [52] W. Kohn, A. D. Becke, and R. G. Parr, "Density functional theory of electronic structure," *Journal of Physical Chemistry*, vol. 100, no. 31, pp. 12 974–12 980, 1996.
- [53] D. McLean, *Grain boundaries in metals*, English. Clarendon Press Oxford, 1957, p. 346.
- [54] J. Greeley and M. Mavrikakis, "Alloy catalysts designed from first principles," *Nature Materials*, vol. 3, no. 11, pp. 810–815, 2004.
- [55] J. L. Rousset, J. C. Bertolini, and P. Miegge, "Theory of segregation using the equivalent-medium approximation and bond-strength modifications at surfaces: Application to fcc Pd-X alloys," *Physical Review B*, vol. 53, no. 8, pp. 4947–4957, 1996.
- [56] M. Ropo, K. Kokko, L. Vitos, J. Kollár, and B. Johansson, "The chemical potential in surface segregation calculations: AgPd alloys," *Surface Science*, vol. 600, no. 4, pp. 904–913, 2006.
- [57] A. V. Ruban, S. I. Simak, P. A. Korzhavyi, and B. Johansson, "Theoretical investigation of bulk ordering and surface segregation in Ag-Pd and other isoelectronic alloys," *Physical Review B*, vol. 75, no. 5, pp. 1–16, 2007.
- [58] M. Polak and L. Rubinovich, "The interplay of surface segregation and atomic order in alloys," *Surface Science Reports*, vol. 38, no. 4-5, pp. 127–194, 2000.

- [59] L. R. Owen, H. Y. Playford, H. J. Stone, and M. G. Tucker, "A new approach to the analysis of short-range order in alloys using total scattering," *Acta Materialia*, vol. 115, pp. 155–166, 2016.
- [60] P. Wynblatt and R. C. Ku, "Surface energy and solute strain energy effects in surface segregation," *Surface Science*, vol. 65, no. 2, pp. 511–531, 1977.
- [61] S. Zafeirotos, S. Piccinin, and D. Teschner, "Alloys in catalysis: Phase separation and surface segregation phenomena in response to the reactive environment," *Catalysis Science and Technology*, vol. 2, no. 9, pp. 1787–1801, 2012.
- [62] H. H. Brongersma, M. Draxler, M. de Ridder, and P. Bauer, "Surface composition analysis by low-energy ion scattering," *Surface Science Reports*, vol. 62, no. 3, pp. 63–109, 2007.
- [63] F. J. Kuijers and V. Ponec, "The surface composition of PdAg alloys," *Journal of Catalysis*, vol. 60, no. 1, pp. 100–109, 1979.
- [64] J. B. Miller, C. Matranga, and A. J. Gellman, "Surface segregation in a polycrystalline Pd₇₀Cu₃₀ alloy hydrogen purification membrane," *Surface Science*, vol. 602, no. 1, pp. 375–382, 2008.
- [65] Z. Li, O. Furlong, F. Calaza, L. Burkholder, H. C. Poon, D. Saldin, and W. T. Tysoe, "Surface segregation of gold for Au/Pd(1 1 1) alloys measured by low-energy electron diffraction and low-energy ion scattering," *Surface Science*, vol. 602, no. 5, pp. 1084–1091, 2008.
- [66] A. Noordermeer, G. A. Kok, and B. E. Nieuwenhuys, "A comparative study of the behaviour of the PdAg(111) and Pd(111) surfaces towards the interaction with hydrogen and carbon monoxide," *Surface Science*, vol. 165, no. 2-3, pp. 375–392, 1986.
- [67] C. W. Yi, K. Luo, T. Wei, and D. W. Goodman, "The composition and structure of Pd - Au surfaces," *Journal of Physical Chemistry B*, vol. 109, no. 39, pp. 18 535–18 540, 2005.
- [68] P. T. Wouda, M. Schmid, B. E. Nieuwenhuys, and P. Varga, "STM study of the (111) and (100) surfaces of PdAg," *Surface Science*, vol. 417, no. 2-3, pp. 292–300, 1998.
- [69] M. Zhao, W. G. Sloof, and A. J. Böttger, "Modelling of surface segregation for palladium alloys in vacuum and gas environments," *International Journal of Hydrogen Energy*, vol. 43, no. 4, pp. 2212–2223, 2018.
- [70] G. H. Vurens, F. C. Van Delft, and B. E. Nieuwenhuys, "The influence of ordering on the surface composition and surface site distribution of binary alloys as studied with the Monte Carlo method," *Surface Science*, vol. 192, no. 2-3, pp. 438–456, 1987.
- [71] M. Ropo, K. Kokko, L. Vitos, and J. Kollár, "Segregation at the PdAg(111) surface: Electronic structure calculations," *Physical Review B*, vol. 71, no. 4, pp. 1–6, 2005.
- [72] L. Vitos, A. V. Ruban, H. L. Skriver, and J. Kollar, "The energetics of steps on transition metal surfaces," *Philosophical Magazine B*, vol. 78, no. 5-6, p. 487, 1998.
- [73] I. Galanakis, G. Bihlmayer, V. Bellini, N. Papanikolaou, R. Zeller, S. Blügel, and P. H. Dederichs, "Broken-bond rule for the surface energies of noble metals," *Europhysics Letter*, vol. 58, no. 5, p. 751, 2002.
- [74] S. Ouannasser, J. Eugène, H. Dreysse, C. Wolverton, and D. de Fontaine, "Study of surface segregation and order in AgPd alloys," *Surface Science*, vol. 307-309, pp. 826–831, 1994.
- [75] S. M. Foiles, "Summary Abstract: Calculation of the surface segregation of Pd–Cu, Pd–Ag, and Pd–Au alloys," *Journal of Vacuum Science & Technology A: Vacuum, Surfaces, and Films*, vol. 5, no. 4, pp. 889–891, 1987.
- [76] M. Zhao, J. C. Brouwer, W. G. Sloof, and A. J. Böttger, "Surface segregation of Pd–Cu alloy in various gas atmospheres," *International Journal of Hydrogen Energy*, vol. 45, no. 41, pp. 21 567–21 572, 2020.
- [77] J. Creuze, H. Guesmi, C. Mottet, B. Zhu, and B. Legrand, "Surface segregation in AuPd alloys: Ab initio analysis of the driving forces," *Surface Science*, vol. 639, pp. 48–53, 2015.
- [78] F. Gao, Y. Wang, and D. W. Goodman, "CO Oxidation over AuPd(100) from ultrahigh vacuum to near-atmospheric pressures: CO adsorption-induced surface segregation and reaction kinetics," *Journal of Physical Chemistry C*, vol. 113, no. 33, pp. 14 993–15 000, 2009.
- [79] V. Soto-Verdugo and H. Metiu, "Segregation at the surface of an Au/Pd alloy exposed to CO," *Surface Science*, vol. 601, no. 23, pp. 5332–5339, 2007.

- [80] G. Hetzendorf and P. Varga, "Preferential sputtering and surface segregation in Au-Pd alloys," *Nuclear Instruments and Methods in Physics Research*, vol. 18, pp. 501–503, 1987.
- [81] D. G. Swartzfager, S. B. Ziemecki, and M. J. Kelley, "Differential Sputtering and Surface Segregation: the Role of Enhanced Diffusion.," *Journal of Vacuum Science & technology*, vol. 19, no. 2, pp. 185–191, 1981.
- [82] S. Nayeboossadri, J. Speight, and D. Book, "Effects of low Ag additions on the hydrogen permeability of Pd-Cu-Ag hydrogen separation membranes," *Journal of Membrane Science*, vol. 451, pp. 216–225, 2014.
- [83] A. Rochefort, M. Abon, P. Delichère, and J. C. Bertolini, "Alloying effect on the adsorption properties of Pd₅₀Cu₅₀(111) single crystal surface," *Surface Science*, vol. 294, no. 1-2, pp. 43–52, 1993.
- [84] A. Noordermeer, G. A. Kok, and B. E. Nieuwenhuys, "Comparison between the adsorption properties of Pd(111) and PdCu(111) surfaces for carbon monoxide and hydrogen," *Surface Science*, vol. 172, no. 2, pp. 349–362, 1986.
- [85] D. Priyadarshini, P. Kondratyuk, Y. N. Picard, B. D. Morreale, A. J. Gellman, and J. B. Miller, "High-throughput characterization of surface segregation in Cu xPd_{1-x} alloys," *Journal of Physical Chemistry C*, vol. 115, no. 20, pp. 10 155–10 163, 2011.
- [86] F. Cheng, X. He, Z. X. Chen, and Y. G. Huang, "Kinetic Monte Carlo simulation of surface segregation in Pd-Cu alloys," *Journal of Alloys and Compounds*, vol. 648, pp. 1090–1096, 2015.
- [87] M. A. Newton, S. M. Francis, and M. Bowker, "Copper-palladium alloy surfaces," *Surface Science*, vol. 259, no. 1-2, pp. 56–64, 1991.
- [88] J. Loboda-Cackovic, M. S. Mousa, and J. H. Block, "Surface analysis of the PdCu(110) single crystal alloy at different segregation rates," *Vacuum*, vol. 46, no. 2, pp. 89–96, 1995.
- [89] B. C. Khanra and M. Menon, "Role of adsorption on surface composition of Pd-Cu nanoparticles," *Physica B: Condensed Matter*, vol. 270, no. 3-4, pp. 307–312, 1999.
- [90] M. S. Mousa, J. Loboda-Cackovic, and J. H. Block, "Characterization of PdCu(110) single crystal surface compositions during CO chemisorption," *Vacuum*, vol. 46, no. 2, pp. 117–125, 1995.
- [91] C. Gallis, B. Legrand, A. Saúl, G. Tréglia, P. Hecquet, and B. Salanon, "Competition or synergy between surface segregation and bulk ordering: The Cu-Pd system," *Surface Science*, vol. 352-354, pp. 588–591, 1996.
- [92] S. Helfensteyn, J. Luyten, L. Feyaerts, and C. Creemers, "Modelling surface phenomena in Pd-Ni alloys," *Applied Surface Science*, vol. 212-213, pp. 844–849, 2003.
- [93] L. V. Poyurovskii, A. V. Ruban, I. A. Abrikosov, Y. K. Vekilov, and B. Johansson, "Application of the Monte Carlo method to the problem of surface segregation simulation," *JETP Letters*, vol. 73, no. 8, pp. 415–419, 2001.
- [94] A. C. Michel, L. Lianos, J. L. Rousset, P. Delichère, N. S. Prakash, J. Massardier, Y. Jugnet, and J. C. Bertolini, "Surface characterization and reactivity of Pd₈Ni₉₂ (111) and (110) alloys," *Surface Science*, vol. 416, no. 1-2, pp. 288–294, 1998.
- [95] P. Miegge, J. L. Rousset, B. Tardy, J. Massardier, and J. C. Bertolini, *Pd₁Ni₉₉ and Pd₅Ni₉₅: Pd surface segregation and reactivity for the hydrogenation of 1, 3-Butadiene*, 1994.
- [96] L. Vitos, A. V. Ruban, H. L. Skriver, and J. Kollár, "The surface energy of metals," *Surface Science*, vol. 411, no. 1-2, pp. 186–202, 1998.
- [97] A. P. Sutton, *Electronic Structure of Materials*, 2004th ed. New York: Oxford University Press, 1993, pp. 174–178.
- [98] H. Jia, A. Goldbach, C. Zhao, G. R. Castro, C. Sun, and H. Xu, "Permeation and in situ XRD studies on PdCuAu membranes under H₂," *Journal of Membrane Science*, vol. 529, pp. 142–149, 2017.
- [99] C. Yin, Z. Guo, and A. J. Gellman, "Surface Segregation across Ternary Alloy Composition Space: Cu_xAu_yPd_{1-x-y}," *Journal of Physical Chemistry C*, vol. 124, no. 19, pp. 10 605–10 614, 2020.

- [100] J. Galipaud, M. H. Martin, L. Roué, and D. Guay, "Pulsed Laser Deposition of PdCuAu Alloy Membranes for Hydrogen Absorption Study," *Journal of Physical Chemistry C*, vol. 119, no. 47, pp. 26 451–26 458, 2015.
- [101] A. M. Tarditi, C. Imhoff, F. Braun, J. B. Miller, A. J. Gellman, and L. Cornaglia, "PdCuAu ternary alloy membranes: Hydrogen permeation properties in the presence of H₂S," *Journal of Membrane Science*, vol. 479, pp. 246–255, 2015.
- [102] A. M. Tarditi, C. Imhoff, J. B. Miller, and L. Cornaglia, "Surface composition of PdCuAu ternary alloys: A combined LEIS and XPS study," *Surface and Interface Analysis*, vol. 47, no. 7, pp. 745–754, 2015.
- [103] M. Zhao, J. C. Brouwer, W. G. Sloof, and A. J. Böttger, "Surface Segregation of Ternary Alloys: Effect of the Interaction between Solute Elements," *Advanced Materials Interfaces*, vol. 7, no. 6, pp. 1–9, 2020.
- [104] A. M. Tarditi, F. Braun, and L. M. Cornaglia, "Novel PdAgCu ternary alloy: Hydrogen permeation and surface properties," *Applied Surface Science*, vol. 257, no. 15, pp. 6626–6635, 2011.
- [105] C. Yu, S. Liao, and H. Deng, "The Rh influence on the surface distribution of the ternary alloy Pt-Pd-Rh," *Applied Surface Science*, vol. 253, no. 14, pp. 6074–6079, 2007.
- [106] J. Luyten and C. Creemers, "Surface segregation in ternary Pt-Pd-Rh alloys studied with Monte Carlo simulations and the modified embedded atom method," *Surface Science*, vol. 602, no. 14, pp. 2491–2495, 2008.
- [107] S. M. Aspera, R. L. Arevalo, H. Nakanishi, and H. Kasai, "First principles study of surface stability and segregation of PdRuRh ternary metal alloy system," *Surface Science*, vol. 671, pp. 51–59, 2018.
- [108] D. N. Tafen, J. B. Miller, Ö. N. Dogan, J. P. Baltrus, and P. Kondratyuk, "Oxygen-induced Y surface segregation in a CuPdY ternary alloy," *Surface Science*, vol. 608, pp. 61–66, 2013.
- [109] R. Boom and F. de Boer, "Enthalpy of formation of binary solid and liquid Mg alloys – Comparison of Miedema-model calculations with data reported in literature," *Calphad*, vol. 68, p. 101647, 2020.
- [110] A. R. Miedema, P. F. de Châtel, and F. R. de Boer, "Cohesion in alloys - fundamentals of a semi-empirical model," *Physica*, vol. 100B, no. 1, pp. 1–28, 1980.
- [111] A. P. Gonçalves and M. Almeida, "Extended miedema model: Predicting the formation enthalpies of intermetallic phases with more than two elements," *Physica B: Condensed Matter*, vol. 228, no. 3-4, pp. 289–294, 1996.
- [112] B. Zhang and W. A. Jesser, "Formation energy of ternary alloy systems calculated by Miedema model," *Physica B: Condensed Matter*, vol. 315, pp. 123–132, 2002.
- [113] Y. Ouyang, X. Zhong, Y. Du, Z. Jin, Y. He, and Z. Yuan, "Formation enthalpies of Fe-Al-RE ternary alloys calculated with a geometric model and Miedema's theory," *Journal of Alloys and Compounds*, vol. 416, no. 1-2, pp. 148–154, 2006.
- [114] W. C. Wang, J. H. Li, H. F. Yan, and B. X. Liu, "A thermodynamic model proposed for calculating the standard formation enthalpies of ternary alloy systems," *Scripta Materialia*, vol. 56, no. 11, pp. 975–978, 2007.
- [115] E. Sadeghi, F. Karimzadeh, and M. H. Abbasi, "Thermodynamic analysis of Ti-Al-C intermetallics formation by mechanical alloying," *Journal of Alloys and Compounds*, vol. 576, pp. 317–323, 2013.
- [116] M. S. Mousavi, R. Abbasi, and S. F. Kashani-Bozorg, "A Thermodynamic Approach to Predict Formation Enthalpies of Ternary Systems Based on Miedema's Model," *Metallurgical and Materials Transactions A: Physical Metallurgy and Materials Science*, vol. 47, no. 7, pp. 3761–3770, 2016.
- [117] R. A. Swalin, *Thermodynamics of solids*. John Wiley & Sons, 1972.
- [118] J. Friedel, "Electronic structure of primary solid solutions in metals," *Advances in Physics*, vol. 3, no. 12, pp. 446–507, 1954.
- [119] F. F. Abraham, N.-h. Tsai, and G. M. Pound, "Bond and strain energy effects in surface segregation," *Scripta Metallurgica*, vol. 13, pp. 307–311, 1979.

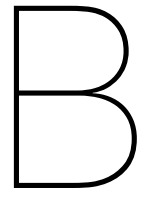
- [120] G. W. Watson, R. P. Wells, D. J. Willock, and G. J. Hutchings, "A comparison of the adsorption and diffusion of hydrogen on the 111 surfaces of Ni, Pd, and Pt from density functional theory calculations," *Journal of Physical Chemistry B*, vol. 105, no. 21, pp. 4889–4894, 2002.
- [121] A. Montoya, A. Schlunke, and B. S. Haynes, "Reaction of hydrogen with Ag(111): Binding states, minimum energy paths, and kinetics," *Journal of Physical Chemistry B*, vol. 110, no. 34, pp. 17 145–17 154, 2006.
- [122] K. C. Chou, "A general solution model for predicting ternary thermodynamic properties," *Calphad*, vol. 19, no. 3, pp. 315–325, 1995.
- [123] G. Kresse and J. Hafner, "Ab initio molecular dynamics for liquid metals," *Physical Review B*, vol. 47, no. 1, pp. 558–561, 1993.
- [124] G. Kresse and J. Furthmüller, "Efficiency of ab-initio total energy calculations for metals and semiconductors using a plane-wave basis set," *Computational Materials Science*, vol. 6, no. 1, pp. 15–50, 1996.
- [125] R. A. Vargas-Hernández, "Bayesian Optimization for Calibrating and Selecting Hybrid-Density Functional Models," *Journal of Physical Chemistry A*, vol. 124, no. 20, pp. 4053–4061, 2020.
- [126] J. P. Perdew, K. Burke, and M. Ernzerhof, "Generalized gradient approximation made simple," *Physical Review Letters*, vol. 77, no. 18, pp. 3865–3868, 1996.
- [127] I. A. Pašti, N. M. Gavrilov, and S. V. Mentus, "Hydrogen adsorption on palladium and platinum overlayers: DFT study," *Advances in Physical Chemistry*, vol. 2011, 2011.
- [128] J.-O. Andersson, T. Helander, L. Höglund, P. Shi, and B. Sundman, "Thermo-calc & dictra, computational tools for materials science," *Calphad*, vol. 26, no. 2, pp. 273–312, 2002.
- [129] B. Sundman, B. Jansson, and J. O. Andersson, "The Thermo-Calc databank system," *Calphad*, vol. 9, no. 2, pp. 153–190, 1985.
- [130] S. A. Cotton and F. A. Hart, "Zirconium and Hafnium," in *The Heavy Transition Elements*. London: Macmillan Education UK, 1975, pp. 3–14.
- [131] T. A. Peters, T. Kaleta, M. Stange, and R. Bredesen, "Hydrogen transport through a selection of thin Pd-alloy membranes: Membrane stability, H₂S inhibition, and flux recovery in hydrogen and simulated WGS mixtures," *Catalysis Today*, vol. 193, no. 1, pp. 8–19, 2012.



Hydrogen adsorption energies

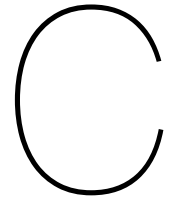
Table A.1: Hydrogen adsorption energies computed using DFT and compared against literature

Element	E_{ads} (eV/atom)		Source
	Literature	This work	
Ag	-0.11	0.24	[29]
Au		0.07	[60]
Co		-0.59	
Cu	-0.21		[29]
Fe	-0.52		[29]
Hf		-1.11	
Ir	-0.48		[29]
La		-0.70	
Mo		-0.89	
Nb		-1.00	
Ni	-0.48	-0.63	[29]
	-0.65		[120]
Pd	-0.48	-0.49	[29]
	-0.48		[127]
	-0.50		[120]
Pt	0.21		[29]
Rh	-0.26		[29]
Ru		-0.55	
Sc		-1.02	
Ta		-1.09	
Ti		-1.11	
V		-1.21	
Y		-0.96	
Zr		-1.00	



Python script for surface segregation

Available on request

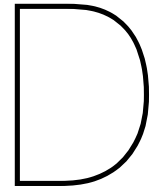


Data required for python script

The file *el_list.csv*, which contains the data required to run the python script to predict surface segregation in ternary alloys. Elements where $A_{lat} = 0$ or $E_H = 0$ are not considered.

Element	V	A	n	ϕ	γ	K	G	at_nr	A_{lat}	E_H
Li	13	5.53	0.98	2.85	0.000525	11	4.2	3	0	0
Be	4.9	2.88	1.67	5.05	0.0027	130	132	4	0	0
Na	23.78	8.27	0.82	2.7	0.00026	6.3	3.3	11	0	0
Mg	14	5.81	1.17	3.45	0.00076	45	17	12	0	0
Al	10	4.64	1.39	4.2	0.00116	76	26	13	4.05	0
K	45.63	12.77	0.65	2.25	0.00013	3.1	1.3	19	0	0
Ca	26.2	8.82	0.91	2.55	0.00049	17	7.4	20	5.58	0
Sc	15.03	6.09	1.27	3.25	0.001275	57	29	21	0	1.02295336
Ti	10.58	4.82	1.52	3.8	0.0021	110	44	22	0	1.11001323
V	8.36	4.12	1.64	4.25	0.00255	160	47	23	3.03	1.214
Cr	7.23	3.74	1.73	4.65	0.0023	160	115	24	0	0
Mn	7.35	3.78	1.61	4.45	0.0016	124	78	25	0	0
Fe	7.09	3.69	1.77	4.95	0.002475	170	82	26	0	0.517624142
Co	6.7	3.55	1.75	5.1	0.00255	180	76	27	0	0.58629645
Ni	6.6	3.52	1.75	5.2	0.00245	180	76	28	3.52	0.476167065
Cu	7.12	3.7	1.47	4.45	0.001825	140	48	29	3.61	0.217060335
Zn	9.17	4.38	1.32	4.1	0.00099	70	43	30	0	0
Y	19.89	7.34	1.21	3.2	0.001125	41	26	39	0	0.95783345
Zr	14	5.81	1.41	3.45	0.002	71	33	40	0	0.995591698

Nb	10.8	4.89	1.64	4.05	0.0027	170	38	41	0	1.005
Mo	9.4	4.45	1.77	4.65	0.003	230	20	42	0	0.89192
Ru	8.2	4.07	1.83	5.4	0.00305	220	173	44	0	0.54518095
Rh	8.3	4.1	1.76	5.4	0.0027	380	150	45	3.8	0.258517412
Pd	8.89	4.29	1.67	5.45	0.00205	180	44	46	3.89	0.476167065
Ag	10.25	4.72	1.36	4.35	0.00125	100	30	47	4.09	0.113417644
Cd	13	5.53	1.24	4.05	0.00074	42	19	48	0	0
Sn	16.3	6.43	1.24	4.15	0.000675	58	18	50	0	0
Sb	16.95	6.6	1.26	4.4	0.000535	42	20	51	0	0
Ba	38.1	11.32	0.81	2.32	0.00037	10	4.9	56	0	0
La	22.55	7.98	1.18	3.17	0.00102	28	14	57	0	0.698551743
Hf	13.45	5.66	1.45	3.6	0.00215	110	30	72	0	1.11001323
Ta	10.81	4.89	1.63	4.05	0.00315	200	67	73	0	1.010516246
W	9.55	4.5	1.81	4.8	0.003675	310	161	74	0	0
Re	8.85	4.28	1.85	5.2	0.0036	370	178	75	0	0
Ir	8.52	4.17	1.83	5.55	0.003	320	210	77	3.84	0.476167065
Pt	9.1	4.36	1.78	5.65	0.002475	230	61	78	3.92	0.217060335
Au	10.19	4.7	1.57	5.15	0.0015	220	27	79	4.08	-0.07313920
Tl	17.23	6.67	1.12	3.9	0.000575	43	2.8	81	0	0
Pb	18.28	6.94	1.15	4.1	0.0006	46	5.6	82	4.95	0
Bi	19.32	7.2	1.16	4.15	0.00049	31	12	83	0	0
Th	19.8	7.32	1.28	3.3	0.00155	54	31	90	5.08	0



Python script to process surface segregation

Available on request